Open Access

Recent Progress in Materials

LIDSEN Publishing Inc.

Original Research

Quantitative Evaluations on Harmonic and Anharmonic Lattice Thermal Capacity of Polymers

Valeri Ligatchev *

Not Affiliated, Singapore 471748, Singapore; E-Mail: lva_singapore@hotmail.com

* **Correspondence:** Valeri Ligatchev; E-Mail: lva_singapore@hotmail.com

Academic Editor: Changming Fang

Recent Progress in Materials
2025, volume 7, issue 2
doi:10.21926/rpm.2502008

Received: December 28, 2024
Accepted: May 14, 2025
Published: May 22, 2025

Abstract

So-called 'Generalized Skettrup Model(s)' (GSMs) of different (1D, 2D, 3D) spatial dimensionalities are used at simulations on temperature-dependent *harmonic* and *anharmonic* fractions of lattice thermal capacity of polyethylene and polypropylene with crystalline and/or amorphous atomic structures of limited spatial extents. Basic equations of the GSM slot in explicitly *quantization effects* of the single-particle and many-particle energy levels of spatially confined phonons. The *harmonic* lattice thermal capacity of 1D and 3D polymers is evaluated entirely based on single-particle (fundamental) states of the confined LA, TA, and optical phonons. Statistical characteristics of many-particle states of the LA and TA phonons are obtained based on the concept of *many-particle* vibrational density-of-states, introduced in 1995. Those characteristics define features of temperature-dependent *anharmonic* lattice capacities of 1D, 2D and 3D versions of the GSM in an essentially 'non-perturbative' manner. *Anisotropic* effects in 3D crystalline polymers are incorporated via evaluation of *anisotropic* sound velocities of conventional thermal waves confined within 3D crystalline fragments of those polymers. Such evaluations have been carried out quantitatively for orthorhombic 3D polyethylene via implementation of the Christoffel Matrix formalism. Simulated temperature-dependent lattice thermal capacities are compared with their experimental counterpart for polyethylene and polypropylene, as well as with predictions of Tarasov's Equations and those of the 'three-band' model.

Keywords
Phonon; confinement; lattice; thermal; capacity; fundamental; harmonic; many-particle; anharmonic

1. Introduction

Intensive experimental and theoretical investigations on the characteristics of thermal capacity of polymers emerged as an important branch of *material science* and *engineering* since 1945 [1-3] (see also references therein). Later, those studies also became an essential research field in *medical* and *biological* sciences [4-6]. Atomic structures of polymers (macromolecules) customarily comprise multiple (though repetitive) chemical units called 'monomers' [6]. In general, polymeric atomic structures may comprise (predominantly) three-dimensional (3D), two-dimensional (2D), or one-dimensional (1D) atomic 'fragments', or a combination of those [1-3]. Graphical representations of the structural units (monomers) of a few well-known polymers with primarily *linear* (1D) spatial structures are sketched in Figures 1(a), 1(b), 1(c), and 1(d).

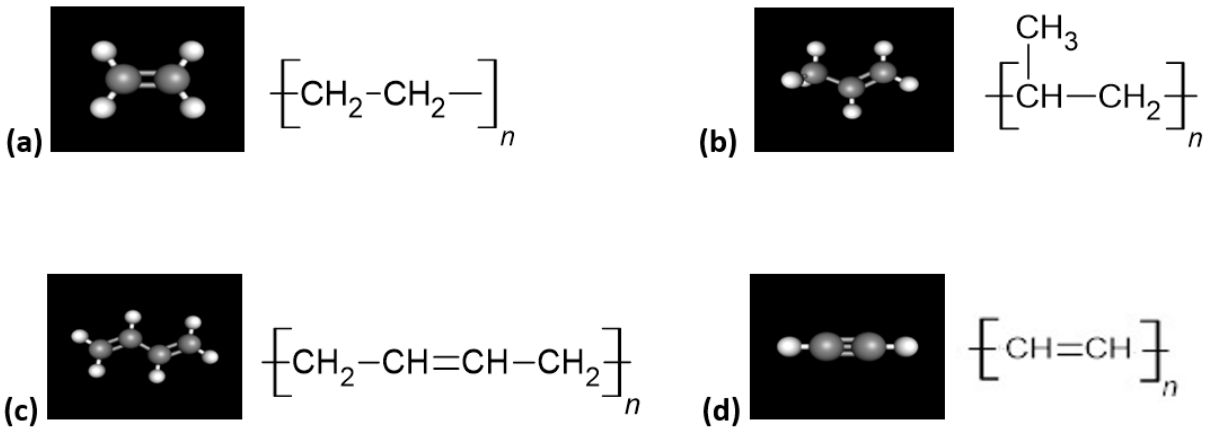

Figure 1 Graphical representation(s) of structural units of **(a)** ethylene/polyethylene, **(b)** propylene/polypropylene, **(c)** butadiene/poly(butadiene) (1,4), and **(d)** acetylene/polyacetylene, with predominantly *linear* molecular arrangements.

Grey balls represent *carbon* atoms, while *white* ones represent *hydrogen* atoms in the graphical illustrations of monomers. The MolView (version 2.4) software is used for the creation of graphical representations of the structural units of *monomers*, while ChemSketch (freeware), version 2.4 (2023), is used for creating sketches of atomic arrangements within all those *polymeric* structural units.

Otherwise, those polymeric structures might also be classified as well based on *spatial connectivity* of its atomic 'network', as 'skeletal' (backbone) fragments, and structural 'groups' [2]; the latter ones might incorporate 'terminal' C-H bonds, as well as 'terminal' CH_3 groups in the atomic structure of polypropylene, see Figure 1(b). Furthermore, the aforementioned polymers and monomers might have (spatially periodic) *crystalline* and/or (spatially disordered) *amorphous* atomic structures, or even their mixture [2]; see also references therein. Those (repetitive) molecular monomeric units themselves apparently form one of the key levels in essentially

hierarchical atomic structures of polymers, with their first (basic) level formed by the (predominantly carbon and hydrogen) atoms composing those monomers.

Higher levels of these 'polymeric' structures could be characterized not only by atomic compositions of the macro-molecules, but also by their *topology* (i.e., spatial 'connectivity' [7] among the adjacent monomers) and *morphology*-i.e., dimensionality, shapes-or 'habit' in terminology of B. Wunderlich [8], -sizes, and crystalline orientation (if any) of molecular fragments (blocks). All these structural, topological, and morphological features of real polymers eventually define their macroscopic characteristics: optical properties, thermal and electrical conductivity, heat capacity, elasticity modulus, etc.

This study is predominantly devoted to comparative descriptions and implementation of several quantitative approaches for simulations on temperature-dependent specific (volumetric) *harmonic* and *anharmonic* lattice *thermal capacities* of a few well-known real polymers. The (isobaric) *specific* thermal (heat) capacity is routinely defined as follows [8, 9]:

$$\mathrm{C_p} = \frac{\partial \mathrm{Q}}{\mathrm{m}\,\partial \mathrm{T}}, \tag{1}$$

here C_p is the isobaric quantity is evaluated at a *constant* environmental *pressure*; ∂Q is the infinitesimally small amount of *heat* (thermal energy) required to increase the absolute temperature, T, of *m* grams of the given material by the infinitesimally small ∂T quantity. Similarly, the *isochoric* heat capacity could be evaluated as well at a *constant volume* of the material, and this quantity is routinely denoted as C_v. The latter heat capacity is traditionally associated with purely *harmonic* contributions from *fundamenta*l (and essentially *single-particle*) states of conventional (i.e., longitudinal and transverse) acoustic phonons, while the C_p quantity is commonly expected to take into account fraction(s) of either '*quasi-harmonic*' or truly *anharmonic* contributions as well [9]. Aforementioned *quasi-harmonic* contributions are customarily associated with '…effects of thermal expansion against a bulk modulus…', while *truly anharmonic* effects '…originate from *interactions* of thermally-excited phonons with other phonons, or from interactions of phonons with electronic excitations…' [9]. Both the C_p and C_v quantities are *temperature-dependent* in general; thus, they could be denoted as $C_p(T)$ and/or $C_v(T)$ functions as well. Typical examples of the *experimental* $C_p(T)$ dependencies, reported for the *polyacetylene* (PA) in ref. [10] and for *polypropylene* (PP) in ref. [11], composed predominantly of with *linear* macromolecules, are plotted in Figures 2(a), 2(b), respectively.

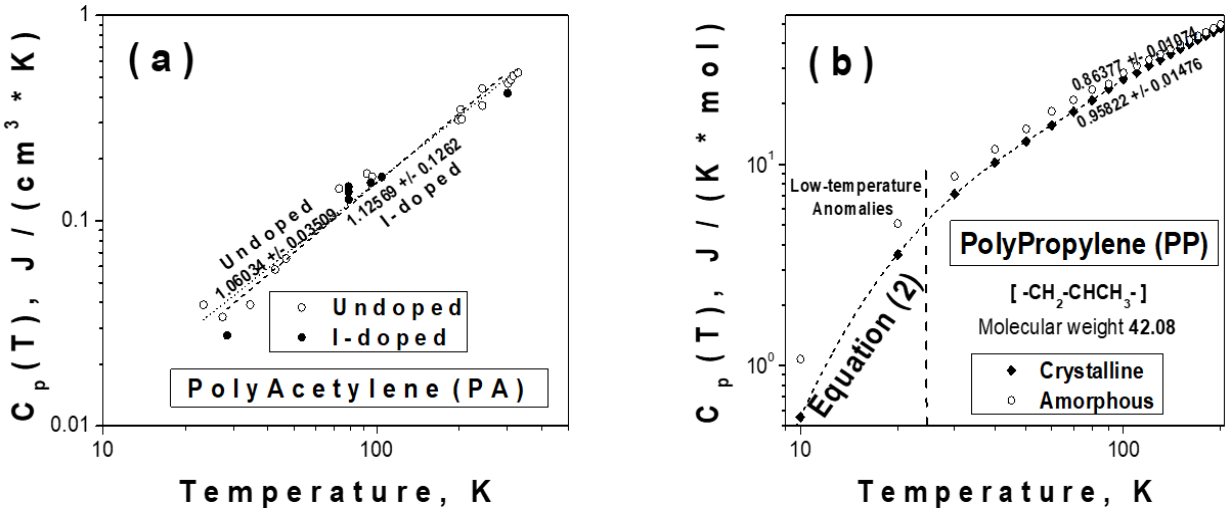

Figure 2 The *experimental* $C_p(T)$ dependencies (symbols) plotted **(a)** for the nominally-undoped and iodine-doped samples of polyacetylene (PA) [10] (see the Figure 5 therein), as well as **(b)** for the amorphous and crystalline modifications of *polypro-pylene* (PP) [11]; the latter figure plotted based on the data, revealed in the Table 4, Table 5 (respectively) of the ref. [11]. Log-log slope(s) of those dependencies, evaluated using standard least-square-fit procedure in the temperature range of (25 K ≤ T ≤ 300 K) for the panel **(a)**, and in the range of (100 K ≤ T ≤ 150 K) for panel **(b)**, are revealed near to the corresponding data sets in both panels. The temperature range corresponding to the 'low-temperature anomalies' is shown in Figure **(b)** as well. The dashed curve in Figure **(b)** corresponds to Equation (3) in ref. [11]; see also Equation (2) herein.

It is noteworthy that the experimental data plotted in Figure 2(a) replicates Figure 5 from the ref. [10]; the appropriate data from that figure is obtained (picked up) using *Plot Digitizer 2.6.8* freeware, created by Joseph A. Huwaldt in 2015 (see also http://plotdigitizer.sourceforge.net), while all points exhibited in Figure 2(b) are plotted based on the data, tabulated (in Table 4 and Table 5) for the case of crystalline and amorphous modifications (respectively) of the *polypropylene* in ref. [11]. As it is seen readily from the Figures 2(a), 2(b), the (relatively) low-temperature $C_p(T)$ function(s) of *linear* PA and PP *macromolecules* apparently *do not follow* the well-known Debye's 'law' [12], $C_p(T) \propto T^3$, which was established firmly for the *bulk* crystalline and amorphous solids at relatively low temperatures.

Instead, experimental $C_p(T)$ function(s) both for the PA and PP macromolecules rather become fairly close to *linear* ones, $C_p(T) \propto T$, (see Figures 2(a), 2(b)), within the temperature range of (100 K ≤ T ≤ 200 K), which is generally expected for the *lattice* heat capacity of 1D structures based on the well-known $C_p(T) \propto T^{(d/r)}$ 'rule' [8], with *dimensionality* of the system *d*, and the (integer) factor *r* in the phonon dispersion dependence: $\omega \propto \mathbf{q}^r$; here ***q*** stands for the phonon quasi-wave vector.

Thus, particularities of the Vibrational Density-of-States (VDOS) become of key importance among other factors outlining $C_p(T)$ behavior of the bulk, spatially non-homogeneous and low-dimensional semiconductors and insulators. Indeed, at $d = r = 1$, $C_p(T) \propto T$ are anticipated for the 1D (linear) macromolecules with *linear* (Debye's) dispersion for the LA and or TA phonons, and the experimental $C_p(T)$ data plotted (re-plotted) in the Figures 2(a), 2(b) follow this 'trend' indeed with an accuracy of ±16% in general (or of ±13% for *crystalline* modifications of PA and PP) within

temperature range of (100 K ≤ T ≤ 200 K). Similarly, (almost) linear $C_p(T)$ dependencies have also been reported for the poly-isobutylene and poly-1-bytene elsewhere in ref. [13], as well as for the linear polyethylene [14] (PE, see its structural 'model' in Figure 1(a)) for the temperature range of (80 K ≤ T ≤ 200 K), see also Figure 3(a) herein.

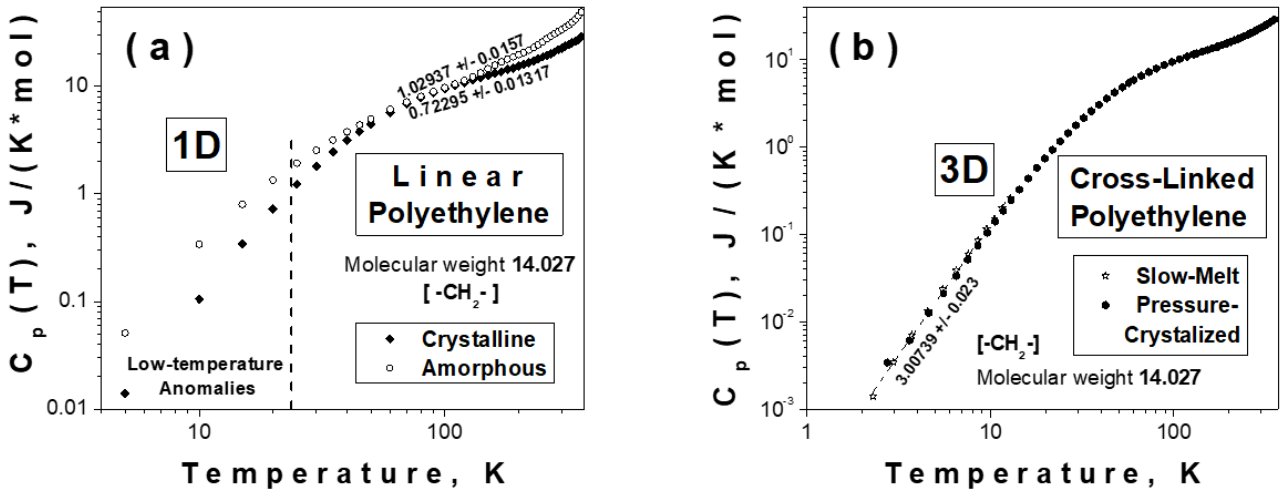

Figure 3 The *experimental* $C_p(T)$ dependencies (symbols) reported for poly-ethylene (PE) in ref. [14]. The Figure **(a)** shows $C_p(T)$ dependencies obtained for amorphous and crystalline modifications of *linear* PE (see Table 1 in ref. [14]), while Figure **(b)** reveals the $C_p(T)$ dependencies, obtained for the 'high-density' PE (HDPE) samples with '*branched*' 3D molecular structure (see Table 2 in ref. [14]). The log-log slope(s) of those dependencies, evaluated using standard least-square-fit procedures in the temperature range of (80 K ≤ T ≤ 250 K in Figure **(a**) and 2 K ≤ T ≤ 20 K in Figure **(b)**), are revealed near to the corresponding curves in both panels. The temperature range corresponding to so-called 'low-temperature anomalies' is shown in Figure **(a)** as well.

In general, the $C_p(T) \propto T$ dependence might also originate from a dominant *electronic* (hole) contribution to the (low-temperature) specific heat capacity of polymeric samples with significant concentration(s) of nearly-free electrons and holes [8, 9]. However, there is *no* (experimental) *data* on either the electronic component of the heat capacity nor on electric conductance, chemical potential (Fermi energy), etc., for the *particular samples* of 1D and 3D polymers, studied elsewhere in refs. [10, 11, 13, 14]. Therefore, *direct* comparison of the electronic and lattice contributions to the experimentally obtained $C_p(T)$ quantities becomes quite *impossible*, while 'indirect' estimations would be somewhat *speculative* and quite confusing.

Besides, in general, the *electronic contribution* to the heat capacity is expected to be *significant* only for polymeric materials with sufficiently *high concentrations* of free electrons (holes), like doped polyaniline (PANI). At the same time, the majority of polymers are well-known dielectrics (insulators) [8, 9]. Those highly conductive polymers are simply out of focus in this article. Furthermore, even for the iodine-doped (I-doped) PA, exhibited elsewhere in ref. [10], potentially *significant* contribution to the $C_p(T)$ function from the nearly-free charge carriers, created due to incorporation of the iodine (I) atoms into atomic structure of the polyacetylene, does *not amend considerably* neither the $C_p(T)$ quantities of I-doped PA, nor its (nearly) linear (in general) character: see features of $C_p(T)$ dependencies plotted in Figure 2(a). This indicates the *dominant* contribution

from the lattice heat capacity to the experimental $C_p(T)$ dependence, reported elsewhere in refs. [11-13] for (predominantly) *linear* macromolecules and other such macromolecules, studied in refs. [15-18]. Thus, within a certain level of simplification(s) (e.g., *ignoring* completely the effect of the *periodic* Born-von Kármán boundary condition [19, 20], temperature-dependent lattice heat capacity of *linear* molecules is widely expected to obey the $C_p(T) \propto T$ 'rule').

It is noteworthy as well that the dashed curve in Figure 2(b) corresponds to the following fitted (within the temperature range of 10 K ≤ T ≤ 100 K) 'empirical' Equation (3) in ref. [11]:

$$C_p(T) = exp[0.241028(\ln T)^3 - 3.01364(\ln T)^2 + 13.5529(\ln T) - 18.7621], \qquad (2)$$

where the $C_p(T)$ quantity is expressed in [J/(mol * K)] units, while the absolute temperature, T, is expressed in Kelvins.

On the other hand, the 'low-temperature anomalies' in temperature ranges of (5 K ≤ T ≤ 25 K) emerge clearly as well for both those structural modifications of *linear* PP (see Figure 2(b)) and PE (see Figure 3(a)). In contrast, 'branched (i.e., 'cross-linked' and predominantly 3D in its atomic network topology) molecular structure of so-called 'high-density' PE (HDPE) samples emerges in the 'canonical' Debye's $C_p(T) \propto T^3$ dependencies for the temperature range (5 K ≤ T ≤ 50 K) [14]: see also Figure 3(b). Thus, an amendment in the structural dimensionality, *d*, of the polymer would have a direct effect indeed on its vibrational spectrum: compare Figures 4(a) and 4(b). Secondly, as it will be discussed in detail in the next section, alterations in *sizes* (spatial extents) of macro-molecules might significantly affect as well the low-temperature parts of experimental $C_p(T)$ dependencies of polymeric solids of different spatial dimensionalities.

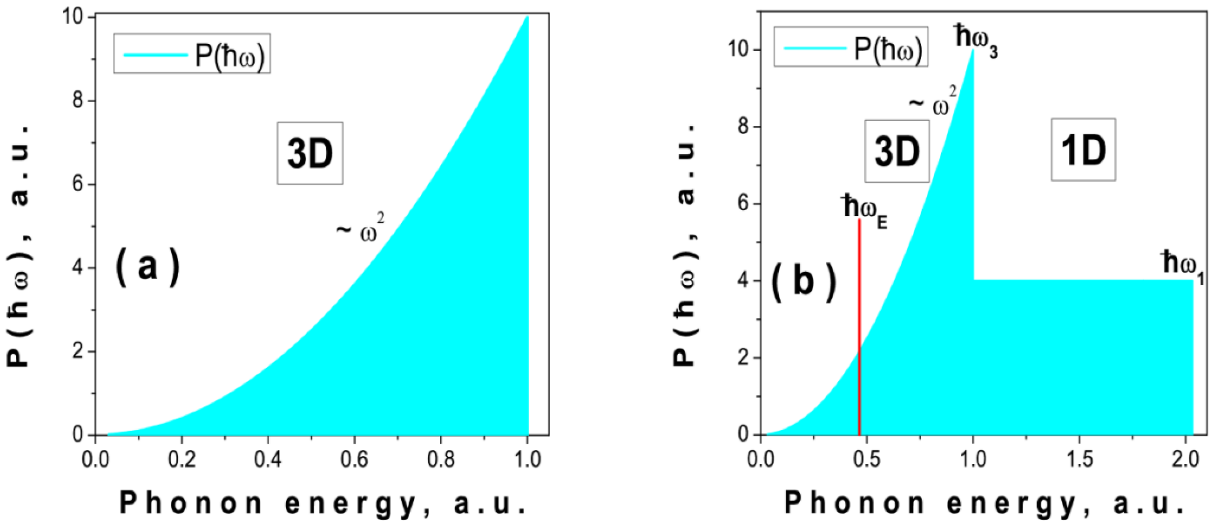

Figure 4 (color online). Idealized fundamental acoustic phonon spectra of **(a)** 3D polymeric structure [12], and of **(b)** polymeric structure composed of 1D and 3D structural fragments (blocks). The latter figure replicates (with some minor amendments) so-called '3-band' model', depicted elsewhere in Figure 5(b) from ref. [18]. The $\hbar\omega_E$ in this picture denotes an (optical) vibrational mode with an Einsteinian spectrum. In contrast, $\hbar\omega_3$ and $\hbar\omega_1$ denote top frequencies of the bands of the thermal acoustic vibrations of the 3D and 1D structural fragments, respectively. Those $\hbar\omega_3$ and $\hbar\omega_1$

quantities could also be linked to the corresponding specific temperatures, θ_3 and θ_1, defined as: $\theta_3 = \hbar\omega_3/k_B$; $\theta_1 = \hbar\omega_1/k_B$. See the main text for more details.

As mentioned above in this section, atomic structures of such polymeric solids often comprise simultaneously 1D, 2D, and/or 3D structural fragments. In such a case, appropriate description of their $P(\hbar\omega)$ function(s) might also requires implementation of a (linear) combination ('super-position') of $P(\hbar\omega)$ dependencies corresponding to the structural fragments of different spatial dimensionalities [18]; see also reference therein and illustration for this statement in Figure 4(b).

Both Equation (2) above and the mentioned above generic $C_p(T) \propto T^{(d/r)}$ 'rules' are customarily matching merely for the relatively *narrow temperature ranges* (usually located *well below* the Debye's temperature of the material) of the experimentally evaluated $C_p(T)$ dependencies of (polymeric) solids of different spatial dimensionalities.

More comprehensive description of the $C_v(T)$ (rather than the $C_p(T)$) dependencies could be obtained using the framework of so-called 'Tarasov's Equations '(TEs)' [1-3]. For instance, the temperature-dependent $C_v(T)$ function for a 'chain' structure is generally expected to obey the 1D version of those TEs [2, 15-17]:

$$\frac{C_v(T)}{3R} = D_1\left(\frac{\theta_1}{T}\right), \tag{3}$$

with

$$D_1\left(\frac{\theta_1}{T}\right) = \left(\frac{T}{\theta_1}\right)\int_0^{\theta_1/T} \frac{\left(\frac{\theta}{T}\right)^2 exp\left(\frac{\theta}{T}\right)}{\left[exp\left(\frac{\theta}{T}\right)-1\right]^2} d\left(\frac{\theta}{T}\right), \tag{3a}$$

where the θ_1 quantity defines highest allowed vibrational temperature (frequency) of the 1D chain (see Figures 4(a), 4(b) and caption to them), while the 3D version of TE reads:

$$\frac{C_v(T)}{3R} = D_3\left(\frac{\theta_3}{T}\right), \tag{4}$$

where

$$D_3\left(\frac{\theta_3}{T}\right) = 3\left(\frac{T}{\theta_3}\right)^3\int_0^{\theta_3/T} \frac{\left(\frac{\theta}{T}\right)^4 exp\left(\frac{\theta}{T}\right)}{\left[exp\left(\frac{\theta}{T}\right)-1\right]^2} d\left(\frac{\theta}{T}\right). \tag{4a}$$

Here $D_1(\theta_1, T)$ and $D_3(\theta_3, T)$ represent in fact (slightly re-formulated) one- and three-dimensional 'Debye functions' [15-17], while the θ_1, and θ_3 quantities are their respective 'frequency' limits (or characteristic temperatures; see Figures 4(a), 4(b), and caption to them) [2, 17], whereas *R* is the 'universal gas constant'. Equation (4a) represent well-known (though re-formulated in terms of actual and 'critical' temperatures only) Debye's equation for the heat capacity of 3D bulk solids [12], and 'covers' quite a wide temperature range, corresponding to both 'incremental' and 'saturating' parts of entire $C_v(T)$ dependencies. Similar equations have also been re-formulated for different

spatial dimensionalities: see Equations (3, 4c) herein and refs. [2, 15-17]. In particular, the following 2D TE had been proposed for the 'layer structures' [2, 17] with the appropriate 2D 'Debye function':

$$D_2\left(\frac{\theta_2}{T}\right) = 2\left(\frac{T}{\theta_2}\right)^2 \int_0^{\theta_2/T} \frac{\left(\frac{\theta}{T}\right)^3 exp\left(\frac{\theta}{T}\right)}{\left[exp\left(\frac{\theta}{T}\right) - 1\right]^2} d\left(\frac{\theta}{T}\right). \qquad (4b)$$

It is noteworthy that synthesis and applications of 2D polymers recently became really 'hot topics' in physics and chemistry of polymers and low-dimensional solids in general due to their unique (sometime-truly *exceptional*) mechanical, thermal, and optical properties [21, 22]. However, the latter TE takes in to account only contributions from 'in-plane' TA and LA modes of (polymeric) 2D layers. In contrast, so-called '*out-of-plane*' ones are *not taken* into account by Equation (4b), though they make a *dominant* impact(s) on the *low-temperature* $C_p(T)$ and $C_v(T)$ functions of 2D materials [23-25]; see also references therein. Yet another vital term within the TE framework is its Einstein's term [17]:

$$\frac{C_{v,E}(T)}{N_E R} = \left(\frac{\theta_U}{\theta_U - \theta_L}\right)\left[D_1\left(\frac{\theta_U}{T}\right) - \frac{\theta_L}{\theta_U} D_1\left(\frac{\theta_L}{T}\right)\right], \qquad (5)$$

here θ_L and θ_U are 'low' and 'upper' temperature (frequency) limits of distributed uniformly (or 'boxed' [8]) vibrational density-of-states, while N_E stands for the total number of atoms involved in the Einstein's mode vibrations [17]. For the Einstein term, $\theta_L \rightarrow \theta_U = \theta_E$ has to be assumed; see also refs. [2, 17] for the comprehensive list of Tarasov's equations of different spatial dimensionalities. It is important, that different forms of TEs (see, for instance, the Equations (4a, 5) above) allow-in principal-the following significant simplifications [26]:

$$C_{v,E}(T) = N_E R \frac{\left(\frac{\theta_E}{T}\right)^2 exp\left(\frac{\theta_E}{T}\right)}{\left[exp\left(\frac{\theta_E}{T}\right) - 1\right]^2} = \frac{N_E R}{4}\left(\frac{\theta_E}{T}\right)^2 csch^2\left(\frac{\theta_E}{2T}\right), \qquad (5a)$$

It is noteworthy as well, that all TEs, expressed by the Equations (3-5a) above could be formulated as well for a more specific situation(s), which, for instance, might comprise of a case when the spectrum of linear (chain) molecules does *not commences* from *zero frequency*, but rather from some *positive* θ_L quantity, forming a 'rectangular' band(s) (or 'boxes' [8]), within a temperature range limited (again) by the θ_L and θ_U quantities [15-17].

Such situation is actually illustrated in Figure 4(b), (which depicts essential features of the '3-band model' [18]) where $\theta_L = \theta_3 = \hbar\omega_3/k_B$, and $\theta_U = \theta_1 = \hbar\omega_1/k_B$, are assumed for 1D vibrations. In such a case, contribution (to the lattice heat capacity) from 1D vibration(s) is expected to be express by the following form of TEs [15-17]:

$$\frac{C_v(T)}{3R} = D_1\left(\frac{\theta_1}{T}\right) - \left(\frac{\theta_3}{\theta_1}\right)\left[D_1\left(\frac{\theta_3}{T}\right) - D_1\left(\frac{\theta_1}{T}\right)\right], \qquad (6)$$

with the $D_1(\theta_1, T)$ and $D_1(\theta_3, T)$ terms expressed by the Equation (3a).

$$D_n\left(\frac{\theta}{T}\right) = n\left(\frac{T}{\theta}\right)^n \int_0^{\theta/T} \frac{x^{n+1}exp(x)}{[exp(x)-1]^2}dx = n\left(\frac{T}{\theta}\right)^n \int_0^{\theta/T} \frac{x^{n+1}}{4} csch^2\left(\frac{x}{2}\right)dx\,. \quad (7)$$

The squared *hyperbolic cosecant* (0.25 * *csch(x/2)*) function(s) [27] in Equations (5a, 7) replaces the combination of the following terms: exp(x)/[exp(x) - 1]^2, within the TEs expressed by Equations (3-5). Based on the following well-known identity: *csch(x/2)* = 1/*sinh(x/2)* [27], even further simplification becomes viable, with $x = (\hbar\omega/k_BT)$; the $\hbar\omega$ standing here for *vibrational* (*phonon*) *energy*, and k_B for the Boltzmann constant. Due to those substitutions (s), the volumetric specific heat of a solid from a *single vibrational* mode (of the frequency of $\hbar\omega_E$) might be expressed as follows [26]:

$$C_v(\hbar\omega_E, T) = k_B \frac{\left(\frac{\hbar\omega_E}{2k_BT}\right)^2}{\left[sinh\left(\frac{\hbar\omega_E}{2k_BT}\right)\right]^2}. \quad (8)$$

This generic term replaces the appropriate TE for the single-mode contribution to $C_v(T)$ quantity, see, in particular, Equations (5, 5a) above. The [*csch(x/2)*] and [1/*sinh(x/2)*] hyperbolic functions in Equations (5a, 7, 8) *diverge* as their argument, $x = (\hbar\omega/k_BT)$, approaches *zero* (i.e., in the $x \rightarrow 0$ limit) [26]. In the context of evaluation on temperature dependencies of the heat capacity of solids of different spatial dimensionalities, the *vanishing x* quantities might emerge either:

(a) in the $T \rightarrow \infty$ limit (which is of no physical *significance* for real solids), and/or

(b) at *infinitesimally small* vibrational energy (i.e., in the $\hbar\omega \rightarrow 0$ limit).

The latter situation (strictly speaking) might emerge within the TEs formalism for the *bulk* solids of (formally) *infinite* spatial extension(s) (sizes) of different spatial dimensionalities. In particular, the {exp(x)/[exp(x) - 1]^2 → 0.25**csch^2(x/2)*} substitution *does not* really *work* for the 1D, and 2D solids of *infinite* spatial extent(s). This eventually implies that the majority of the listed above TEs would *not allow* such *substitution* due to *divergence* in the *csch(x/2)* and [1/*sinh(x/2)*] functions in the $\hbar\omega \rightarrow 0$ limit. Nonetheless, for *bulk* 3D solids, the aforementioned substitution emerges in physically meaningful results. Indeed, within the framework of Debye's (classical) approximation, the $P(\hbar\omega) \propto (\hbar\omega)^2$ is generally expected for the *long-wavelength* vibrations within bulk 3D solids [12]. Thus, since *csch^2(x/2)* ∝ (2/*x*)^2, for *infinitesimally small x* quantities, the [$P(\hbar\omega)$ *csch^2*($\hbar\omega$/2)] product would eventually yield just a *finite* (low-temperature) $C_v(T)$ quantity in the $\hbar\omega \rightarrow 0$ limit. However, since the $P(\hbar\omega) \propto (\hbar\omega)$ is expected for 2D solids within the long-wavelength limit, and the $P(\hbar\omega)$ function is expected to be *phonon-energy-independent* in this limit for 1D solids, their product with the *csch^2(x/2)* function would *diverge* in the $x \rightarrow 0$ limit: the [$P(\hbar\omega)$ *csch^2*($\hbar\omega$/2)] function would diverge as ~$(1/\hbar\omega)$ for 2D solids at $\hbar\omega \rightarrow 0$ limit, and as ~$(1/\hbar\omega)^2$ for 1D ones of (formally) *infinite* spatial extent in the same limit. On the other hand, the aforementioned divergence problem might be avoided *naturally,* due to the *phonon confinement* phenomenon and related to it 'infra-red' gap in the phonon spectra, for the polycrystalline, microcrystalline, and especially for *nano-crystalline* solids of different spatial dimensionalities, as well as for their amorphous and/or amorphous-crystalline counterparts. Nevertheless, even the framework of 3D TEs customarily does not depict yet another significant feature of *experimental low-temperature* $C_p(T)$ dependencies, obtained for

different kinds of real polymers of finite spatial extents. In particular, so-called 'low-temperature anomalies' emerge clearly for experimental $C_p(T)$ dependencies, obtained for 1D, 2D, and 3D spatially non-homogeneous solids; typical cases of such 'anomalies' are shown in Figure 2(b) and Figure 3(a).

Indeed, $C_p(T)$ dependencies in these figures *diminish* rapidly with the temperature decrement below $T \cong 30$ K for both amorphous and crystalline modifications of PP. These 'anomalies' are intimately related to the specific features (i.e., infra-red 'cut-offs') of the phonon spectra of those *linear* macromolecules. For instance, the (1D-in this particular case) phonon *confinement* effect would originate 'discretization' in the allowed energies of those phonons, and open the 'gap' as well in the 'bottom' of the spectra of the confined LA and TA phonons [23-25, 28]. Thus, briefly discussed above in this section *quasi-continuous* $P(\hbar\omega)$ function(s) (see Figures 4(a), 4(b) for illustration), which is customarily obeying the $P(\hbar\omega) \propto (\hbar\omega)^{d-1}$ 'rule' for the vibrational spectra of polymeric solids have to be replaced with its 'discretized' counterpart (as it is illustrated schema-tically in Figure 5 for the '3-band model' case), when the 'critical' spatial *extent* (size) of the solid becomes well *comparable* with its (average) interatomic distance. Therefore, instead of *horizontal line*, representing the vibrational spectrum of a 1D structural fragment (of formally infinite length) in Figure 4(b), we should rather expect a set of *vertical lines* (representing Dirac's δ-functions), separated on the horizontal scale by the (phonon) energy gap(s) of $\Delta E_{1D} \equiv E_{min} = (2hc_s/L_z)$; here E_{min} stands for the 'minimal' vibrational energy of spatially confined 1D vibrations [28], see right-hand side of Figure 5. At $c_s = 15000$ m/s and $L_z = 100$ nm this equation yields: $\Delta E_{1D} \cong 1.24$ meV.

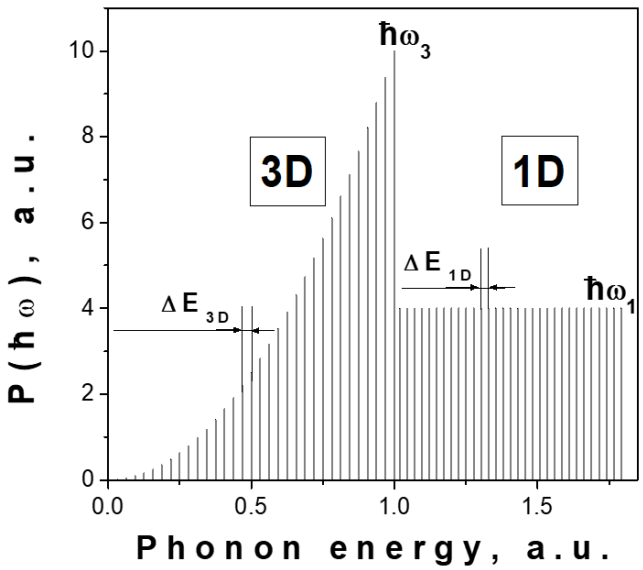

Figure 5 More realistic representation (though not to scale) of fundamental acoustic phonon spectra of a polymeric structure composed of 1D and 3D structural fragments (blocks) of *limited* spatial extents. The quantization effects of acoustic modes confined within those structural blocks originate separation(s) between the phonon energy levels, which apparently become 'discrete' in such a case, with the separation (gap) energies of ΔE_{1D}, and ΔE_{3D}, respectively. See for comparison the original '3-band' model [18] depicted in Figure 4(b) above and other details in the main text.

Such energy gap(s) *diminish* in vibrational spectra of 1D MWs (inversely proportionally) with the L_z *enlargement* and formally *completely vanish* in the $L_z \rightarrow \infty$ limit. Similarly, the separation (gap) among neighboring vibration levels of the rectangular 2D and parallelepipedal 3D structures would be defined by appropriate algebraic combinations of the (effective) sound velocities of the material(s), and (orthogonal) spatial extents of those structures [25, 29]. Further discussion(s) on the physical origin(s) and particular features of those $P(\hbar\omega)$ and $C_v(T)$ functions within the relatively low phonon energy and temperature ranges for polymeric solids of different morphologies and spatial dimensionalities would be unveiled in the next section.

Yet another important feature of experimental $C_p(T)$ dependencies of real polymeric solids is (potentially) significant contributions from *anharmonic* effects, especially at elevated temperatures. The *temperature-dependent* (in general) difference among the C_p and C_v quantities of 3D materials could be (formally) linked to the coefficient of the *volumetric thermal expansion*, α_v, [24, 30]:

$$C_p^0 - C_v^0 = V_0 B_T T \left[\alpha_v^2 + \left(\int_0^T \alpha_v dT \right) \left(\frac{d\alpha_v}{dT} \right) \right], \qquad (9a)$$

where C_p^0 is an *isobaric* heat capacity of a solid at a *zero pressure*, C_v^0 is its *isochoric* (harmonic) counterpart, measured at *zero temperature*, V_0 is a 'molar volume' of a solid at T = 0, while B_T is its so-called isothermal 'bulk modulus', $B_T = -V_0 * (\partial P/\partial V_0)|_T$ [23, 29, 30]. The *ratio* of the B_T quantity to its *isochoric* counterpart, B_v, is routinely defined via the following ratio: $[C_p(T)/C_v(T)]$; which is very close (within accuracy of ~0.1%) to *unity* for majority of solids at relatively low temperature, T. Therefore, the B_T quantity is expected to be (roughly) equal to the B_v one.

For *cubic crystals* (of diamond atomic structure), the B_v quantity is routinely defined as follows: $B_v = (c_{11} + 2c_{12})/3$, where c_{11} and c_{12} denote two (of four independent) *elastic constants* (components of *elastic tensor*) of those crystal(s) [29, 30], see also references therein. For a 3D material with a *temperature-independent* volume expansion coefficient, α_v, the latter *integral equation* could be simplified to the following *algebraic* one [29, 30]:

$$C_p^0 - C_v^0 = V_0 B_T T \alpha_v^2. \qquad (9b)$$

It is noteworthy that Equations (9a, b) are based essentially on the assumption of validity of '*quasi-harmonic*' approximation for a given 3D solid [8, 29, 30]. Therefore Equations (9a, b) predict *linear* enlargement of the in $C_p(T)$ quantities with the temperature at the *constant* (temperature-independent) α_v quantity, $C_p(T) \propto T$, for the temperatures, T, well exceeding the Debye's temperature of the 3D solid, where the $C_v(T)$ dependence usually 'saturates' based on prediction of the well-known Debye's model [12] for the specific (volumetric) thermal capacity of bulk solids.

For *low-dimensional* (i.e., 1D, 2D) solids, the coefficient of the *volume* thermal expansion has to be replaced with its low-dimensional *counterpart*(s): i.e., with the *linear* and '*areal*' thermal expansion coefficient(s), respectively. Such a replacement would cause amendments in the Equations (9a, b). However, this kind of amendment(s) would require using the appropriate low-dimensional 'bulk modulus' of 1D and 2D materials [31-34]. Such elastic modulus (i.e., their 'low-dimensional' counterparts) *is not well-defined* for the 2D and especially for 1D materials. However, a more detailed discussion on this issue is given elsewhere in the refs. [35-37]; see also references therein. Therefore, implementations of Equations (9a, b) at quantitative evaluations on *anharmonic*

and/or *quasi-harmonic* fractions of (lattice) thermal capacity of low-dimensional solids become infeasible.

There is also some controversy regarding appropriate computational methodology, even at quantitative evaluations on the *harmonic* thermal capacity of *oligomers*: solid and (especially) liquid polymers comprising just a few 'repetitive' units [38]. As it was suggested in ref. [38]. The specific heat of a solid comprising the *only* vibrational mode might be evaluated appropriately based on Equation (8) above in this section; see also Equations (3) in ref. [38] and ref. [39] for more details. For relatively small structural units of oligomers, the quantum confinement effect is generally expected to be of apparent significance for 1D, 2D, and 3D cases. In particular, it would *eliminate* all potential *divergence problems* with the integrand of appropriate TEs—nevertheless, the essentially classical (i.e., obtained *without* considering *quantum effects*) approach presented in refs. [38, 39] is based on (classical version of) molecular dynamics (MD) simulation methodology and 'mass-weighted velocity' autocorrelation function [39], and it has been implemented elsewhere in ref. [38] at simulations on temperature dependencies of lattice thermal capacities of oligomers. Such methodology requires quantum *corrections* due to the presence of hydrogen atoms and/or 'terminal groups' in the atomic structures of polymers: (thermal) motions of such atoms have to be treated in an essentially quantum manner, which customarily is *not incorporated* into the 'classical' MD methodology [38]. Quantum nature of those nuclear degrees of freedom might be treated within the 'path-integral' framework [38]. However, this approach is computationally demanding [38, 40].

More practical ways of computational corrections might be based on the so-called '*Wigner-Kirkwood* expansion' [41, 42]. However, it is essentially 'classical' in its nature, as well as still computationally challenging, and valid for a limited temperature range only, which does not cover absolute temperatures well below Debye's one [38, 41, 42], and-in particular-the temperature range of aforementioned 'low-temperature anomalies'. Furthermore, this technique does *not capture* the aforementioned generic quantum mechanical, and especially *anharmonicity* effect(s) [38]. Herein, the 1D, 2D and 3D versions of so-called 'Generalized Skettrup Model' (GSM) [23-25, 28, 29] (see also references therein), representing 'alternative' (as compared to approximations, mentioned above in this section) and *fully quantized* computational approaches will be implemented at simulations on temperature dependencies of lattice thermal capacities of few polymers of different spatial dimensionalities and morphological characteristics. However, before it, the fundamental equations of the 1D, 2D and 3D versions of the GSM will be re-introduced briefly in the *next section*.

2. Basic Equations of GSMs

The *isochoric* lattice heat capacity of 3D *bulk* polymeric solids of (formally) *unlimited* spatial extents (sizes) is customarily defined by the one-dimensional integration over their *quasi-continuous static* (and usually *temperature-independent*) vibrational (phonon) spectrum, $P(\hbar\omega)$, 'weighted' by the (temperature-dependent) Bose-Einstein occupation factor for those vibrational states, and by the (appropriate) phonon energy, $\hbar\omega$ [12]. Within the framework of the (original) Debye's model, all (static) states of the longitudinal and transverse (LA, TA) acoustic phonons are presumed to obey *linear* (classical) dispersion(s) [12].

Spatial extents of 'morphological units' (e.g. crystallites of various shapes, cylindrical, spherical and conical non-homogeneities, etc.) of 3D *polycrystalline*, spatially *non-homogeneous amorphous* [23, 43] and especially those of the nano-structured solids [24] are *limited* by definition for all of them. Under (Casimir's) assumption on *insignificant* phonon-phonon interactions (scattering) within volumes of those non-homogeneities (morphological units), propagation length (*mean free path*) of their LA and TA phonons would be defined by the *sizes* (spatial extents) of those morphological units [24, 29] rather than by phonon-phonon interactions. This allows one to treat volume(s) of the single morphological unit (3D cavity) as the actual volume of *spatial confinement* (coherence) of the (static) LA and TA vibrational states [24, 29]. Since neighboring energy levels of *confined* LA and TA phonons are generally expected to be *separated* from each other [43], alteration in the morphological characteristics of the polycrystalline and spatially non-homogeneous amorphous solids might originate considerable re-distribution in the energies (spectrum) of the confined LA and TA vibrations [24, 29]. Therefore, spectral and statistical characteristics of those LA and TA phonon states confined within the 3D units (cavities) are generally expected to be affected by their morphology i.e., *shapes* (or 'habit' [8]): e.g., parallelepipedal, cylindrical, conical, etc., of those non-homogeneities, as well as by their sizes and (dominant) crystalline orientation(s)-if any [24, 29, 43]. Thus, in general, the temperature-dependent lattice thermal capacities of spatially non-homogeneous and especially of the low-dimensional solids are expected to be affected by their morphology [24].

2.1 Basic Equations of 1D GSM

Within framework of 1D version of the 'Generalized Skettrup Model' (GSM) the temperature-dependent lattice thermal capacities of *infinitesimally thin* (in both spatial directions, *orthogonal* to the MW elongation) 1D 'Molecular Wires' (MWs) of a *finite* length, L_z, is defined by the following expression [28, 44]:

$$C_p^{1DGSM}(T) \cong \frac{1}{k_B T^2} \sum_{N=1}^{N_M} \sum_{p=1}^{Np_{max}} \frac{exp\left(p\frac{E_{min}}{k_B T}\right)}{\left[exp\left(\frac{pE_{min}}{k_B T}\right)-1\right]^2} \frac{(pE_{min})^2}{N!\,(Z_{1D}^N)} \left[floor\left(\frac{L_z}{a_l N}\right)\right]^N, \qquad (10)$$

where the function *floor(x)* returns an integer part of its *rational* argument, a_l is an (average) *interatomic* distance ('lattice constant') of the MW material, k_B is the Boltzmann constant, E_{min} is the 'minimal' energy of the phonons, confined within 1D MW, Z_{1D}^N is the N-phonon 'statistical sum' (N-particle partition function), while c_{eff} is an *effective* sound velocity, routinely defined as follows: $3/c_{eff} = (1/c_l + 1/c_{t1} + 1/c_{t2})$ [23], where c_l stands for the *longitudinal* sound velocity, while c_{t1} and c_{t2} denote two (different in general) transverse sound velocities of the MW material. The aforementioned E_{min} and Z_{1D}^N quantities are customarily defined as follows [28, 44]:

$$E_{min} = \frac{2hc_{eff}}{L_z}, \qquad (10a)$$

$$Z_{1D}^N = \left[L_z\left(\frac{k_B\theta_D}{hc_{eff}}\right)\right]^N. \qquad (10b)$$

The p_{max} quantity in Equation (10) is defined as: $p_{max} = floor(k_B\theta_D/E_{min})$; where θ_D is Debye's temperature of the MW material [27, 43]. The Equation (10) allows the following simplification, discussed (to some extent) in the previous section: $\{exp(x)/[exp(x) - 1]^2\} \rightarrow 0.25\, csch^2(x/2)$ [26], with the *dimensionless* $x = (\hbar\omega/k_BT) = (pE_{min}/k_BT)$ quantity. Such substitution simplifies Equation (10) till its following form:

$$C_p^{1DGSM}(T) \cong 4k_B \sum_{N=1}^{N_M} \sum_{p=1}^{Np_{max}} \frac{csch^2\left(\frac{pE_{min}}{2k_BT}\right)}{N!\, Z_{1D}^N} \left(\frac{pE_{min}}{2k_BT}\right)^2 \left[floor\left(\frac{L_z}{a_l N}\right)\right]^N . \qquad (10c)$$

The basic equation(s) of the 1D GSM version, formalized by the Equations (10-10c), generally predict *linear* $C_v(T)$ enlargement with the absolute temperature, T, in its *low-temperature* range (where $T << \theta_D$ holds) for sufficiently *long* MWs (see simulation results and detailed discussion on this issue in the next section), though the 'low-temperature' anomalies also emerged clearly for the $C_v(T)$ curves, obtained for relatively short MWs: see, in particular, Figure 2 in ref. [28] as well as Figure 2 in ref. [44]. It is noteworthy as well, that Equations (10, 10c) incorporates not only *harmonic* lattice capacity of MWs (evaluated based on those equation at N ≡ 1), but also its *anaharmonic* fraction(s), evaluated at N = 2, 3, 4…. Further analysis and discussion on features of $C_v(T)$ and $C_p(T)$ dependencies, *evaluated* based on Equations (10-10c) for *linear* polymers (chains) and *oligomers* will be presented in next section.

2.2 Basic Equations of 2D GSM

For instance, the lattice thermal capacity of the *rectangular* 2D nano-ribbons, it is essentially defined by the two following 'components' [22-25]. The 'in-plane' and 'out-of-plane' ones [25]. The former one reads [25]:

$$C_p^{2DGSM}(T) \cong \frac{2}{k_BT^2} \sum_{N=1}^{N_M} \sum_{p=1}^{Np_{max}} \frac{exp\left(p\frac{E_{min}}{k_BT}\right)}{\left[exp\left(\frac{pE_{min}}{k_BT}\right) - 1\right]^2} \frac{(pE_{min})^2}{N!\, Z_{2D}^N} \left[\frac{2\sqrt{2}\kappa p F_2(L_x, L_y)}{N\sqrt{1 + (L_x, L_y)^2}}\right]^N , \qquad (11a)$$

with 'form-factor', $F_2(L_x, L_y)$, equals to $F_2(L_x, L_y) = (\pi/2)$, for the *square* flakes [25], but varying significantly with the (L_x/L_y) ratio for rectangular ribbons: see Figure 1 in ref. [25], while the term $\kappa = (p_{max}/2)[1 + (p_{max}/4)]$ takes into account contribution(s) from *permutation*(s) of appropriated single-phonon state into statistical weigh of the given multi-phonon ones [25]. The 'out-of-plane' contribution reads [25]:

$$C_{ZA}^{2DGSM}(T) \cong \frac{1}{k_BT^2} \sum_{N=1}^{N_M} \sum_{q=1}^{q_{max}} \frac{exp\left(q\frac{E_{min}}{k_BT}\right)}{\left[exp\left(\frac{qE_{min}}{k_BT}\right) - 1\right]^2} \frac{(qE_{min})^2}{Z_{ZA}} \left(\frac{L_xL_yqE_{min}}{\pi\hbar\xi_{ZA}}\right), \qquad (11b)$$

with $q_{max} = p_{max} = floor(k_B\theta_D/E_{min})$, and,

$$E_{min} = \frac{2hc_{eff}}{\left[\left(L_x^2 + L_y^2\right)/2\right]^{1/2}}, \qquad (11c)$$

while the 'statistical sums', $Z_{2D}{}^{N}$, and Z_{ZA}, read [23, 25, 45]:

$$Z_{2D}^{N} = \left[\frac{L_x L_y}{2}\left(\frac{k_B\theta_D}{hc_{eff}}\right)^2\right]^N, \tag{11d}$$

$$Z_{ZA} = \left[\frac{L_x L_y}{2}\left(\frac{\hbar\omega_{ZA}^{M}}{\pi h\zeta_{ZA}}\right)^2\right]. \tag{11e}$$

However, for the *rectangular* ribbons with larger ('microscopic') sizes (spatial extents), the basic equation of a 'quasi-continuous' version of the 2D GSM could implemented as well [23-25]:

$$C_p^{2DGSM}(T) \cong 4k_B C_2 \sum_{N=1}^{N_M} \int_{E_{min}}^{Nk_B\theta_D} \frac{csch^2\left(\frac{E_T}{2k_BT}\right)}{N!\,Z_{2D}^{N}} \frac{E_T^2}{(2k_BT)^2}\left[\frac{2L_xF_2(L_x,L_y)E_T}{Nhc_{eff}}\right]^N dE_T, \tag{11f}$$

with its *size-dependent* 'normalizing coefficient', C_2, defined as follows [23-25]:

$$C_2 = \left[\frac{(k_B\theta_D)^2}{L_xL_y}\right]\left[\frac{L_xL_y}{2\pi^2\left(hc_{eff}\right)^2}\right]^{3/2}. \tag{11g}$$

Mind the $\{exp(x)/[exp(x) - 1]^2\} \rightarrow 0.25\ csch^2(x/2)$ *replacement* [26] in Equation (11f); with $x = (E_T/k_BT)$. Some results of implementations of the basic equations of 2D GSM at simulations on temperature-dependent lattice thermal capacity of 2D polymers have been discussed elsewhere in the refs. [23-25].

2.3 Basic Equations of 3D GSM

The (quasi-continuous though essentially *anisotropic*) *version* of the basic equation of the 3D GSM reads:

$$C_p^{*GSM}(T) \cong 12k_B C_3 \sum_{N=1}^{N_M} \int_{E_{min}}^{Nk_B\theta_D} \frac{E_T^2 csch^2\left(\frac{E_T}{2k_BT}\right)}{N!\,Z_N(k_BT)^2}\left[\frac{2L_xL_y\mathbf{F}\left[\left(\frac{L_x}{c_{efx}}\right),\left(\frac{L_y}{c_{efy}}\right),\left(\frac{L_z}{c_{efz}}\right)\right]E_T^2}{Nh^2c_{efx}c_{efy}}\right]^N dE_T, \tag{12}$$

with the 'orthogonal' components, c_{efx}, c_{efy}, and c_{efz}, of *anisotropic* effective sound velocity, for the phonons (thermal vibrations), confined within the parallelepipedal volume (crystallite) of the orthogonal rib lengths of L_x, L_y, L_z, and the *dimensionless* function, $\mathbf{F}[(L_x/c_{efx}), (L_y/c_{efy}), (L_z/c_{efz})]$, depends solely on the (L_x/c_{efx}), (L_y/c_{efy}), and (L_z/c_{efz}) *ratios*; see also Equation (26b) in ref. [29], and Equation (1) in ref. [46].

Quantitative evaluation on the c_{efx}, c_{efy}, and c_{efy}, values could be, for instance, carried out based on so-called 'Christoffel Matrix' (CM) formalism [24, 29, 46]; see also references therein and further discussion on this issue in the next section. Other key parameters of the Equation (12) are defined as follows [29, 46]:

$$E_{min} = \frac{2h\left[\left(c_{efx}^2 + c_{efy}^2 + c_{efz}^2\right)/3\right]^{1/2}}{\left[\left(L_x^2 + L_y^2 + L_z^2\right)/3\right]^{1/2}}, \tag{12a}$$

$$Z_M = \left[\frac{L_x L_y L_z}{3}\left(\frac{k_B \theta_D}{h c_l^{avr}}\right)^3\right]^M, \tag{12b}$$

$$C_3 = \left[\frac{(k_B \theta_D)^3}{L_x L_y L_z}\right]\left[\frac{L_x L_y L_z}{2\pi^2\left(h c_{ef}^{avr}\right)^3}\right]^{4/3}, \tag{12c}$$

with c_{ef}^{avr} = {[(c_{efx})^2 + (c_{efy})^2 + (c_{efz})^2]/3}$^{1/2}$ [46]. These variant(s) of the basic equations of the *anisotropic version* of the 3D GSM could be, for instance, implemented at quantitative evaluations on temperature-dependent lattice thermal capacity of polyethylene, with significant *anisotropy* in its single-particle vibrational DOS function and sound velocities, see next section for details. It is note-worthy, that statistical characteristics of many-particle states of the LA and TA phonons embedded in all mentioned above versions of the GSM are obtained based essentially on concept of *many-particle* vibrational density-of-states (VDOS), introduced by the author of this article elsewhere in 1995 [47].

2.4 Entropy Calculations

Listed above (just in the *previous* sub-section) basic equations of the 1D, 2D and 3D versions of the GSM have obtained based entirely on quantitative evaluation on the *fundamental vibrational energy* of *acoustic phonons*, *confined* within 1D, 2D, and/or 3D structural fragments of solid polymers, as well as of its *many-particle* counterparts. Another crucially *important* thermodynamic characteristic of the solid polymers is their *entropy* [8, 9]. Indeed, as it was stated by Professor Brent Fultz elsewhere in ref. [9], 'Without entropy to complement energy, thermodynamics would have the impact of one hand clapping.'; please see beginning of the section I.1 of the ref. [9]. In general, the entropy might be evaluated based on the Boltzmann's definition: $S_B = k_B \ln\Omega$ [9], which is mainly determined by the '…number which counts the way of finding of the internal coordinates for thermodynamically-equivalent macroscopic states.', Ω Since the Ω quantity (as well as its natural logarithm) is apparently *dimensionless*, physical dimension of the Boltzmann's entropy is of J/K; i.e., it is the *same* as that of the Boltzmann's constant and of heat capacity (when measured for a unit mass of the substance).

However, more *practical* approach to evaluation on the *temperature-dependent* and *size-dependent* entropy of polymers could be based on an additional 'treatment' of preliminary simulated temperature dependencies of the isobaric *lattice* heat capacity [9]:

$$S_T - S_0 = \int_0^T \frac{C_p(\vartheta)}{\vartheta} d\vartheta, \tag{13}$$

here S_0 stands for the *zero-temperature* (Nernst's) entropy. It is easy to verify that, based on Equation (13), the entropy dimension would be of J/(mol * K) again. Based on the so-called 'third

law' of thermodynamics, $S_0 \equiv 0$ is postulated for the *crystalline solids* with perfectly *ordered* atomic structures, while for amorphous (as well as for majority of polymeric) solids, *positive* S_0 quantities are generally expected [9]. Therefore, Equation (13) would rather yield *relative* changes in the S_T quantities with the temperature. On the other hand, in combination with the Equations (10a-10c, 11a-11f, 12-12c), it might be implemented *straightforwardly* at quantitative evaluation on the entropy of 1D, 2D, and 3D structural fragments (respectively) of polymeric solids. Practical examples of such evaluation(s) for the polymeric materials with clearly dominant 1D and 3D structural fragments would be exhibited and discussed in the next section of the article. At the same time, the $C_p(T)$ quantities taken into account in Equation (13) should *not include electronic* contribution(s): such a contribution is *not related* to the *entropy* of the polymeric *lattice*!

As mentioned above, atomic structure(s) and morphologies (habitats) of real polymers might comprise fragments of different spatial dimensionalities. When (rigid) bounds of such structural fragments are of simple and (essentially) 'convex' geometrical shape (e.g., square, rectangular, cubical, parallelepipedal, etc.), an appropriate combination of the fundamental equations of the 1D, 2D and 3D versions of the GSM (see, in particular, Equations (10-10c, 11a-11d, and 12-12c) above in this section) might be implemented readily at quantitative evaluations on temperature dependencies of thermal capacities of real polymers. However, the composition of fragments of different spatial dimensionalities might result in more complicated morphologies of those polymers. For instance, even 'linear' (chain) polymeric structures of PA and PP might comprise 'MWs' of different lengths. The realistic sketch of a thinkable polymeric 2D morphology might be thought as (approximately) rectangular 2D 'blocks' (of the rib length of L_x^* and L_y^*), though with 'non-rigid' 'corrugated' (e.g., -'concave'-see an example in Figure 6 below) and even 'fractal' borders of the ribbon(s).

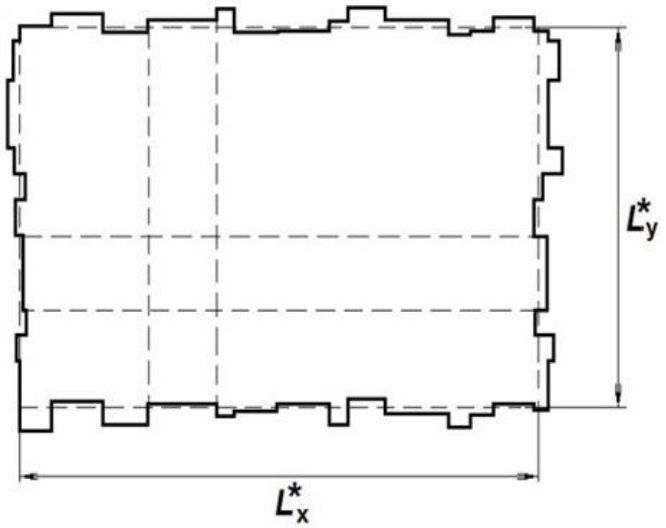

Figure 6 A sketch of an evocative rectangular (ribbon) polymeric 2D morphology with a combination of 'convex' and 'concave' ribbon borders. The (appropriately) averaged (orthogonal) lengths of this ribbon are denoted as L_x^* and L_y^*. In principle, this particular shape could be represented as a 'superposition' of conventional rectangular fragments with 'convex' borders: see dashed lines in the figure. See also more details in the main text.

In such a case, the 'resonant' conditions for (standing) acoustic waves (phonons) might be (somewhat) different (non-equivalent) for various parts of the 2D polymeric fragment. Thus, both eigenenergies of the confined vibrational states as well as *separation* among the neighboring vibrational level(s) spatially confined within a 2D fragment (ribbon) might vary sizably even for different parts of the atomic structures located within such a ribbon. Therefore, appropriate evaluation(s) on the (practical) spatial extents (sizes) and consecutive implementation of basic Equations (11a-11g) at quantitative simulations on the temperature-dependent lattice thermal fragment would require some kind of 'averaging' of the geometrical parameters (sizes) of those 2D fragments with 'concave' ribbon borders.

Alternatively, an 'effective' spatial extent(s) of the phonon confinement could be approximated using the following equation [48]:

$$\Lambda_{eff} = \frac{1 + p_r}{1 - p_r} \Lambda_{Cs}, \tag{14}$$

Here, Λ_{eff} is the 'effective' mean-free-path (MFP) of phonons, p_r is the probability of a phonon to be specularly reflected on the edge of the 2D (and/or 3D) structural fragment of the polymeric structure. Λ_{cs} is the so-called 'Casimir' MFP, evaluated based on the assumption of dominance of phonon scattering on the *borders* of the ribbons (non-homogeneities) as well as on the absence of significant phonon-phonon interactions within each ribbon [48].

The p_r = 0 corresponds to the 'purely diffusive' case, while p_r = 1 corresponds to the 'purely specular one [48]; see also comment to Equation (2) in ref. [48]. Equation (14) had been initially proposed for evaluation on thermal transport parameters of *silicon nano-wires* (SiNWs) with 'corrugated' shapes. Though features of phonon confinement within SiNWs of *cylindrical* morphology in general is expected to be defined by its 3D geometry, *axial symmetry* of SiNW might *reduce* an effective spatial 'dimensionality' of its phonon confinement and diminish and *log-log* slopes of the $C_v(T)$ and/or $C_p(T)$ dependencies within the 'low-temperature' range(s) [28, 44]. However, such a dimensionality reduction and the slope diminishment might *not occur* for SiNWs with 'corrugated' shapes, where the cylindrical symmetry might be 'distorted' considerably. Similarly, an actual shape (habit) of 3D fragments of real polymeric morphology (not shown herein) could be even far more complicated than compared to presumed (within the framework of 3D GSM) parallelepipedal ones. Some predictions on temperature dependencies of the lattice thermal capacity of more realistic structural and morphological models of polymeric materials obtained using an appropriate combination(s) of the basic equations of 1D and 3D versions of the GSM are discussed in the *next section*.

3. Simulation Results and Discussion

Effects of alteration (variation) in the lengths of MWs (presumably) composing a PP-based polymeric solid of (predominantly) 1D-linked atomic structure on temperature dependence of its *isochoric* (harmonic) lattice thermal capacity, $C_v(T)$, are illustrated in Figures 7(a) and 7(b). All simulated $C_v(T)$ dependencies exhibited in these figures are obtained based on combination(s) of Equation (10c), implemented for the case of *PolyPropelene* (PP), with c_{eff} = 2740 m/s [49], a_l = 20.78 Å [8], θ_D = 600 K, and presumably composed of *two* MWs of different *lengths*. In particular, the PP samples with $C_v(T)$ dependencies, revealed in the Figure 7(a) is (presumably) composed of two MWs

of L_z = 4 nm and L_z = 6 nm, incorporated into the same PP sample with equal volume fractions of 50% for each type (lengths) of the MW.

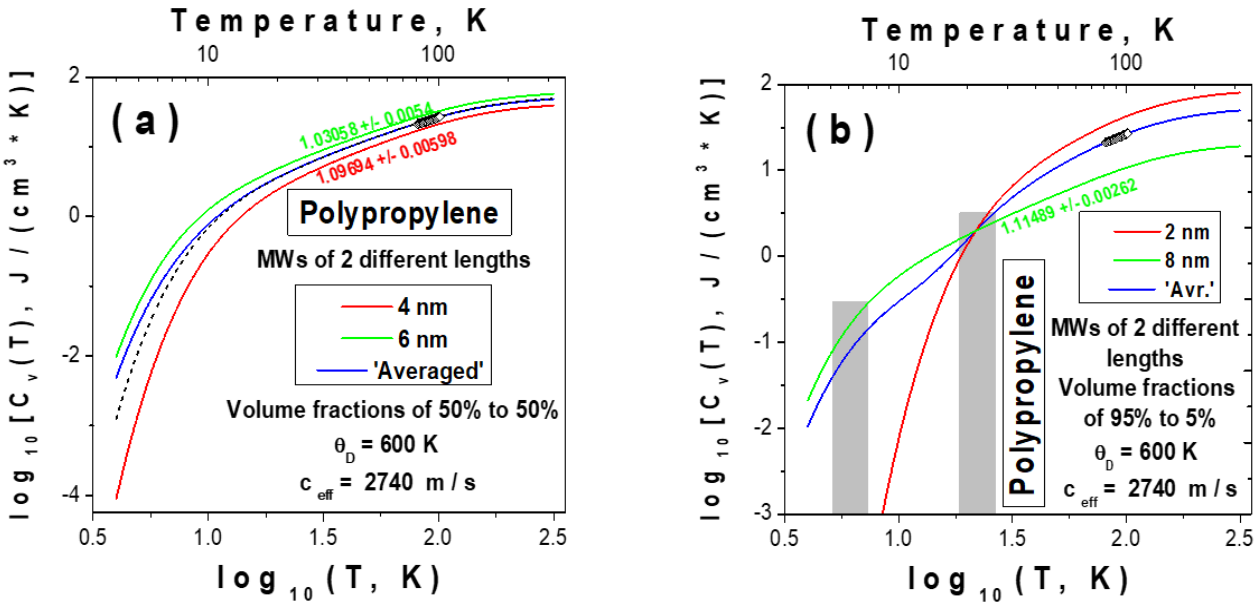

Figure 7 (color online). Curves: simulated temperature dependencies of *isochoric* lattice thermal capacity of PP samples 'composed' of MWs of two essentially *different lengths*: **(a)** of 4 nm and 6 nm (with volume fractions of those MWS of 50% to 50%, respectively) **(b)** of 2 nm and 8 nm (with volume fractions of those MWs of 5% to 95%, respectively). Blue curves in both panels represent linearly 'averaged' (measurable) $C_v(T)$ dependencies for those PP samples, evaluated based on the volume fractions of the two MWs. The dashed black curve in the left panel corresponds to $C_v(T)$ dependence, simulated using Equation (10c) for 'geometrically averaged' MW length; see main text for details. Open symbols: *experimental* $C_p(T)$ data set, replicated (with some 'truncation') from ref. [11], see also Figure 2(b) above. Two grey rectangular(s) on the right panel highlight two distinguishable 'low-temperature anomalies', emerging into the simulated blue curve for the PP samples composed of two MWs of distinctly different lengths. Log-log slopes of a couple of curves, evaluated within a temperature range of (32 K ≤ T ≤ 72 K), are indicated in the close vicinity of those curves.

In contrast, their counterparts revealed in Figure 7(a) are obtained for PP samples (presumably) composed of two MWs of L_z = 2 nm and L_z = 8 nm, incorporated into the PP sample with the volume fractions of 95% and 5%, respectively. Thereafter, the 'averaged' (measurable) $C_v(T)$ dependencies (represented with the *blue* curves in Figures 7(a), 7(b)) are obtained through the linear combination of two 'individual' $C_v(T)$ curves, 'weighted' by their volume fractions. As it seen clearly from comparison of $C_v(T)$ dependencies, plotted in Figures 7(a), 7(b), alteration in lengths of MWs might originate considerable differences in temperature behaviors of those 'averaged' $C_v(T)$ curves, especially in the temperature ranges, corresponding to that of 'low-temperature anomalies'. Indeed, mixture of two MWs with their length of 4 nm and 6 nm would yield the 'averaged' $C_v(T)$ curve with a behavior, very similar to that of individual $C_v(T)$ dependencies, simulated independently for the PP samples (presumably) composed entirely of MWs of the *same lengths*: 4.0 nm (red curve in the Figure 7(a)) and 6.0 nm (green curve in the Figure 7(a)).

The dashed black curve in Figure 7(a)is obtained based on Equation (10c) for the case of 'geometrically averaged' MW length, L_z^*, with $L_z^* = (L_z^1 L_z^2)^{0.5}$, which yields $L_z^* \cong 4.9$ nm at $L_z^1 = 4.0$ nm and $L_z^2 = 6.0$ nm. When, however, lengths difference of the MW 'components' becomes much more distinct (4 times-to be exact), two 'low-temperature' anomalies of such PP sample might emerge in principle at a certain combination of concentrations of MWs, composing the PP sample: see temperature sub-ranges for the 'averaged' (blue) curve, highlighted with *two* grey rectangular(s) in the Figure 7(b). At higher temperatures (i.e., at T > 30 K), the log-log slopes of the simulated $C_v(T)$ curves in Figures 7(a), 7(b), are close to unity (with an accuracy of ±12%), which is generally expected for the temperature-dependent $C_p(T)$ function of the 1D solids with linear phonon disperseon(s) based on the well-known $C_p(T) \propto T^{(d/r)}$ 'rule', discussed briefly in the introductory section.

The temperature dependencies of the entropy, $S_T(T)$, evaluated for the one-dimensional (linear) MWs of polypropylene based on the combination of Equations (10a-10c, 13), are plotted in Figure 8. It is noteworthy, that the simulated $C_v(T)$ dependencies plotted in this figure are obtained based on the *isochoric* $C_v(T)$ curves (i.e., similar to those plotted for the PP samples in Figures 7(a), 7(b)), rather than on their *isobaric* counterparts, $C_p(T)$, embedded into Eq. (13). Such replacement is predominantly enthused by the fact, that the *difference* among the $C_p(T)$ and $C_v(T)$ curves becomes rather *negligible* at relatively low temperatures (at $T << \theta_D$), where amendments in the lengths of the PP MWs effects the simulated $S_T(T)$ dependencies mostly.

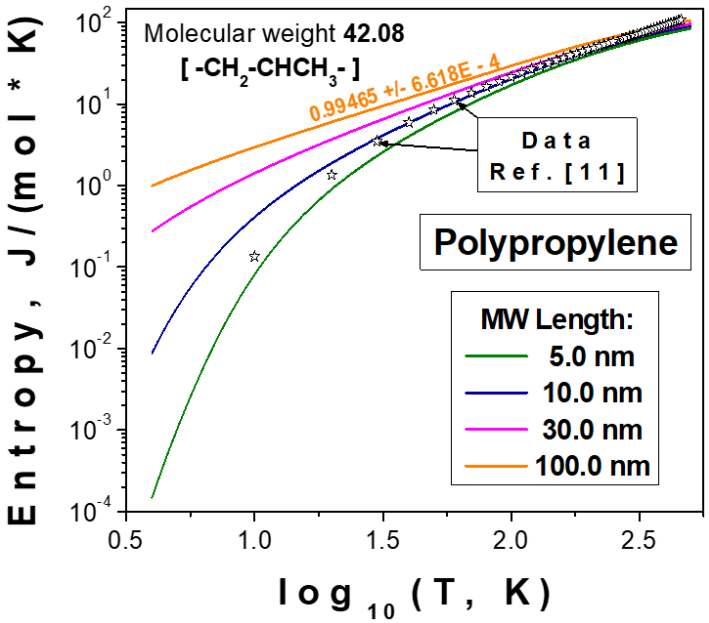

Figure 8 (color online). Curves: simulated (at different lengths of MWs) temperature dependencies of the *relative* entropy of linear PPs. All exhibited simulation results are obtained based on *combinations* of Equations (10a-10c, 13) in the previous section. The $S_T(T)$ dependencies plotted in this figure are actually obtained based on simulated *ishochoric*, $C_v(T)$, dependencies, obtained based on Eq. (10c) for the PPs, rather than on their *isobaric* counterparts, $C_P(T)$, stated in the Eq. (13). Mind *double-logarithm* scales of the plot and close to *linear* behaviour of its upper curve in the temperature range of (10 K ≤ T ≤ 100 K). The $S_T(T)$ data tabulated in Table 4 of the ref. [11] For *crys-talline* PP, plotted for comparison with *open stars*. See the main text for more details.

Indeed, as it is seen readily from Figure 8, alteration in the lengths of PP MWs affects strongly shape of the $S_T(T)$ dependencies within their (5 K ≤ T ≤ 30 K) sub-ranges, where their shape is affected predominantly by the 'low-temperature anomalies' of the simulated $C_v(T)$ dependencies: see, for instance, Figures 7(a), 7(b). It is noteworthy that the simulated $S_T(T)$ curves match fairly well with their experimental counterpart at L_z quantities ranging from 5 to 7 nm: see Figure 8. However, enlargement in the length of the PP MWs weakens anomalous behavior both for the $C_v(T)$ and $S_T(T)$ curves in Figure 7(a) and Figure 8, and aforementioned 'anomalies' (almost) vanish when the MW length exceeds 30 nm. In such a case, the $C_v(T)$ dependence is expected to be close to a *linear* one at relatively low temperatures, and, based on Eq. (13), we also should anticipate the (nearly) linear $S_T(T)$ curve. Indeed, for the *linear* $C_v(T)$ dependence (which is generally expected for the 1D semiconductors and insulators at the relatively low temperatures-see detailed discussion on this issue in the introductory section), a *constant* $[C_v(\theta)/\theta]$ 'integrand' in Eq. (13) emerges-and, consequently-the *linear* $S_T(T)$ curve is apparently anticipated customarily for such a case.

The significant diminishment(s) in the $S_T(T)$ quantities at relatively low temperatures in Figure 8 could also be explained based on Boltzmann's definition of entropy. Indeed, as it was already mentioned above, the 'low-temperature anomalies' are eventually originated from a 'gap' in the low-energy part(s) of the vibrational spectrum of nano-materials. This implies straightforwardly, that the 'number of ways' in which the 'thermodynamically-equivalent' microscopic state(s) of the nano-material could be achieved at the given temperature would be reduced sharply as compared to the similar 'number of ways' for a 'low-temperature' state of its bulk counterpart [9]. This would eventually *diminish* as well the low-temperature Boltzmann's entropy of the nano-structured solids and the measure of their thermally-induced *structural* disorder. However, at higher absolute temperatures, rises of both $C_v(T)$ and $S_T(T)$ curves are slowing down (see Figures 7(a), 7(b), Figure 8)-regardless to the MW length(s), because of the *temperature-independent* numbers of microscopic states occupied at elevated temperatures-which eventually yield deviation from the linear $S_T(T)$ dependencies in Figure 8.

Thus, implementation of the basic equation(s) of the 1D GSM at quantitative evaluation(s) on the temperature dependencies of the *isochoric* lattice thermal capacity of real polymeric solid composed predominantly of 1D MWs of different lengths might provide useful inside into effects of 1D spatial confinement within those MWs on the behavior of the 'averaged' $C_v(T)$ dependencies of the entire PP samples. Moreover, the same equation of the 1D GSM might also be implemented at realistic simulations on the experimental $C_v(T)$ dependencies, obtained from real PP samples, and in combination with Eq. (13) of their temperature-dependent entropy: see Figure 8. As shown in Figure 9(a), the implementation of the *first term* of Equation (10c) from the previous section might replicate convincingly the 'recommended' (in ref. [11]) *isobaric* experimental data for the crystalline modification of PP at $L_z \cong 4.5$ nm. Similarly, simulated $S_T(T)$ dependences for PP approximate reasonably well its experimental counterpart at $L_z = 5 \div 7$ nm, see Figure 8. As it is seen readily from Figure 9(a), within the temperature range (10 K ≤ T ≤ 200 K), the simulated $C_v(T)$ curve follows closely the experimental data for the crystalline modification of PP, reported in ref. [11]. Though it apparently deviates from the data at higher temperatures. In particular, above this temperature range, the simulated $C_v(T)$ (or $C_H(T)$) dependence *underestimates* the experimental trend, obtained for the crystalline modification of PP in ref. [11].

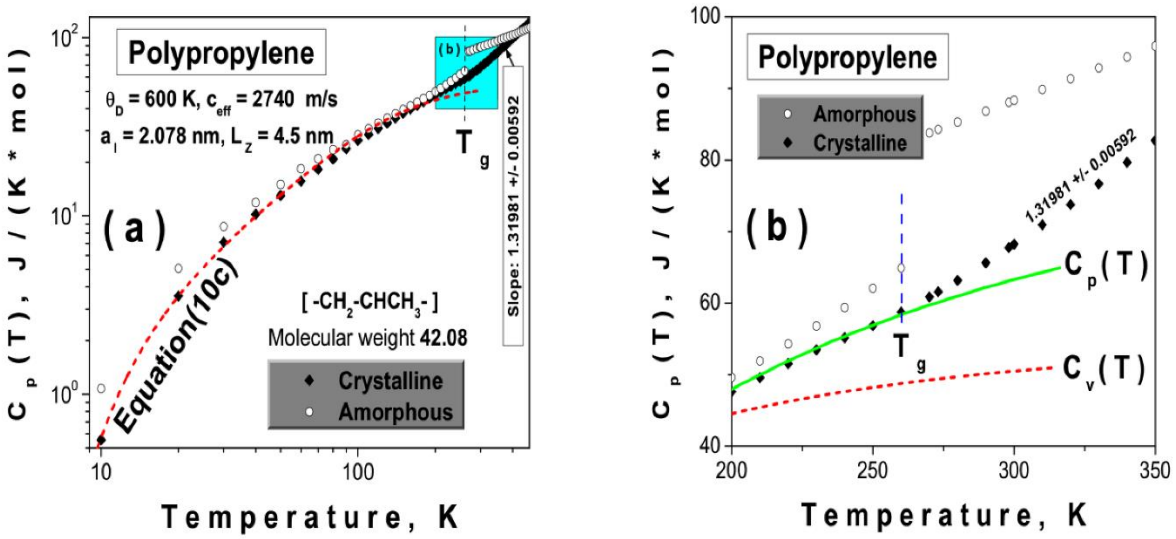

Figure 9 (color online). The experimental (symbols, see also Figure 2(b) above) and simulated (curves) temperature dependence of the isobaric and isochoric lattice thermal capacity of amorphous and crystalline modifications of *linear* polypropylene (PP). Figure **(b)** just 'stretches' the part of Figure **(a)**, highlighted with the cyan rectangular area. All simulated results are obtained based on Equation (10c) in the previous section, both for *harmonic* (at N ≡ 1) and dominant *anharmonic* (at N = 2) fractions of the lattice thermal capacity of 1D (linear) PP. The 'glass transition' temperature, T_g = 260 K [11], of 'atactic' and amorphous modification(s) of PP is indicated with the dashed *vertical line* in both panels. An average log-log-slope for the crystalline modification of the PP, evaluated above the T_g temperature is indicated as well in Figures **(a)** and **(b)**. Mind *double-logarithmic* axes (scales) in Figure **(a)** and *linear* ones in Figure **(b)**. See more details in the main text.

This deviation has to be attributed predominantly to the fact that the very *first term* of Equation (10c) evaluates only the *harmonic* (isochoric) contribution to temperature-dependent lattice thermal capacity of PP, while the impact from the *anharmonic* fraction of the isobaric heat capacity might be significant at the elevated temperature.

In order to take into account the aforementioned *anharmonic* contribution(s) to the experimental *isobaric* $C_p(T)$ quantities, the high-order term(s) of Equation (10c) have to be evaluated as well. In particular, the contribution from the *dominant anharmonic* term (obtained from Equation (10c) at N = 2) becomes significant at elevated temperatures, exceeding 200 K in this particular case; see also simulation results in Figure 2 in ref. [28] and in Figure 2 in ref. [44] for an alternative set of material (simulation) parameters. In general, basic eqation(s) of the 1D GSM predict (almost) *linear increament* with the temperature for both *harmonic* and *anharmonic* fractions of the lattice thermal capacity of MWs within quite a wide temperature range(s) below Debye's temperature of the MW material [28, 44]. However, such a range for the *anharmonic* fraction usually becomes considerably wider due to higher (in general, being proportional to the integer N quantity) summation limits for the anharmonic terms in Equations (10, 10c). Therefore, an appropriate *sum* of the harmonic and dominant anharmonic terms, evaluated based on Equation (10c) for the PP case, eventually yields a reasonably good approximation for the experimental $C_p(T)$ dependence for the crystalline

modification of PP: see the solid curve in Figure 9(b). It is noteworthy that the contribution from the anharmonic *fraction* to the *total* (isobaric) lattice thermal capacity of MWs is *not reflected* (plotted) in Figure 9(a).

Similarly, implementation of the first and second tems of Equation (10c) at simulation(s) on the tempearture dependencies of *harmonic* and *anharmonic* thermal capacity of *amorphous* modification of *linear* polyethylene (PE) yield fairly good approximations at c_{eff} = 2142 m/s, a_l = 2.6 Å [50], θ_D = 900 K, and L_z = 5.8 nm for experimental $C_v(T)$ and/or $C_p(T)$ data, reported elswhere in ref. [14], in quite a wide temperature range: see Figures 10(a), 10(b). Indeed, the first term of Equation (10c) yields a convincing approximation for the experimental $C_p(T)/C_v(T)$ dependence reported for the *linear* PE in ref. [14] Within the temperature range up to 150 K (see Figure 10(a)), while at higher temperatures, the contribution from the *anharmonic* term to the lattice heat capacity of PE MWs becomes significant as well, see Figure 10(b).

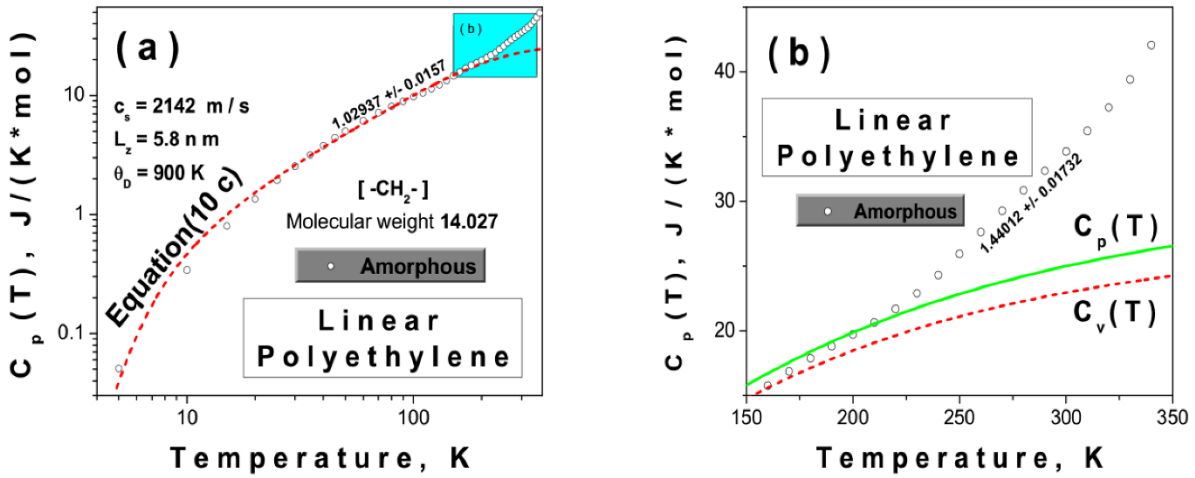

Figure 10 (color online). The experimental (symbols, see also tabulated data in ref. [14], and Figure 3(a) herein) and simulated (curves) temperature dependence of the isobaric and isochoric lattice thermal capacity of *amorphous* modification of *linear* polyethylene (PE). Figure **(b)** actually just 'stretches' the part of Figure **(a)**, highlighted with the cyan rectangle. All simulated results are obtained based on Equation (10c) in the previous section both for *harmonic* (simulated at N ≡ 1) and dominant *anharmonic* (simulated at N = 2) fractions of the lattice thermal capacity of 1D (linear) PE. Material parameters for linear PE are chosen based on the data revealed in refs. [8, 50]. An average log-log slope for the *amorphous* modification of the linear PE, evaluated within temperature range (80 K ≤ T ≤ 250 K) is indicated as well Figure **(a)**, while similar slope in the Figure **(b)** is evaluated for the temperature range of (250 K ≤ T ≤ 325 K). Mind *double-logarithmic* axes (scales) in Figure **(a)** and *linear* ones in Figure **(b)**. See more details in the main text.

Hence, comparison of the experimental $C_p(T)$ and $S_T(T)$ data reported for both *crystalline* and *amorphous* modifications of linear PP and PE elsweher in refs. [11, 14] (respectivelly), and replicated herein in Figures 8, 9(a)-10(b), with the $C_p(T)/C_v(T)$ simulation(s) carried out based on the first (*harmonic*) and second (dominat *anharmonic*) terms of Equation (10c),-in combination with Eq.(13) for $S_T(T)$ evaluations-proves validy of those equations for quite realistic approxi-mation of temperature-dependent harmonic and anharmonic fractions of the lattice thermal capa-city the

essentially 1D polymeric materials (composed mainly of MWs). However, further enlargement in the absolute temperature of those 1D polymeric materials causes significant deviations even of the simulated $C_p(T)$ and $S_T(T)$ dependencies from their experimental counter-parts. Indeed, as it is seen readily from the Figure 9(a), and Figure 10(b), high-temperature log-log slope(s) of experi-mental $C_p(T)$ dpendencies deviate significantly from the *unity* (which is generally expected for the polymers with the *linear* molecular structures and MWs [8]): such slope becomes equal to ~1.32 for the *crystalline* modification of PP above T ≅ 260 K (see Figure 9(a)), while it approximately equlas to ~1.44 for the *amorphous* modification of PE above T ≅ 250 K (see Figure 10(b)). Such deviations of the experimental $C_p(T)$ results from the simulated curves obtained based on Equation (10c) could be attributed both to implementation of a 'truncated' (by its just two dominant terms) version of this equation, as well as by (somewhat) *simplified* version of the entire Equation (10c) itself. Indeed, in general, as it was mentioned elsewhere in ref. [25], complete set of the confined vibrational many-particle (*anharmonic*) states of LA and TA phonons have to incorporate essentially *permutations* of their fundamental states (or so-called 'Fock states' [51]) with all available (for the given system) quantities of single-phonon energy, while all *anharmonic* states incorporated into Equation (10c) are 'composed' merely on (algebraic) products of their single-phonon states of the *same* energy [28, 44]. However, such modifications of the Equation (10c) would not be introduced and analyzed herein, though similar modifications are reflected in the basic equation of the 2D GSM: see Equation (3) of ref. [25]; and Equation (11a) herein.

Nevertheless, in this study, we do *not implement* the aforementioned 2D equations for any kind of simulations on the temperature-dependent thermal capacity of 2D polymeric materials, predominantly due to the lack of reliable experimental $C_p(T)$ data for those 2D polymers. On the other hand, earlier versions of (quasi-continuous and/or 'discretized') basic equations of 2D GSM have already been used at simulation(s) on the $C_v(T)$ and $C_p(T)$ functions for square flakes and rectangular ribbons off graphene, hexagonal boron nitride, molybdenum and tungsten disulfides [23-25]. Those simulations were carried out taking into account explicitly contributions from both 'in-plane' and 'out-of-plane' components of the harmonic and/or *anharmonic* fractions of confined 2D lattice thermal vibrations [23-25].

As for 3D *anisotropic* version of the basic equation(s) of the GSM, exhibited in the previous section (see also references therein), they might be implemented at simulation(s) on $C_v(T)$ and $C_p(T)$ dependencies for 'cross-linked' polymers with substantially 3D topology of molecular network. As it was argued elsewhere in ref. [52], The spatial characteristic of thermal transport in so-called 'high-density' polyethylene (HDPE) is essentially *anisotropic*, which implies the necessity of implementing the anisotropic version of the basic equation of the 3D GSM at appropriate simulations on isochoric and isobaric lattice thermal capacity of this polymeric material. However, that basic equation requires the orthogonal components, c_{efx}, c_{efx}, and c_{efx}, of the *effective* sound speed of PE as equation parameters. Since reference literature data on this quantities in PE is quite controversial (in particular the group and/or phase sound velocities of PE may vary in the range from approximately of 1.35 km/s to approximately of 17 km/s [53]; see also references therein), it would be more appropriate to evaluate it in a more reliable way based on so-called 'Christoffel Matrix' (CM) formalism [28, 44, 54].

The CM, Γ_{ij}, for the *non-piezoelectric* solid reads [54]:

$$\Gamma_{ij} = \frac{l_{iK} c_{KL} l_{Lj}}{\rho_M}, \tag{15}$$

Here, l_{KL} is the 'propagation direction' matrix, c_{KL} is the *elastic stiffness constants matrix*, while ρ_M stands for mass density of (polymeric) solid. The c_{KL} matrix manifests a *compact representation* of the fourth-rank 'stiffness tensor' [54]. In general, the *elastic stiffness constants matrix* is of the sizes 6 × 6, and comprises of 36 elements, and could be obtained for *crystalline solids* with atomic structures of *every known* symmetry class (*Bravais lattice*) [54]. The CM approach is based essentially on simplifying assumptions on *linear* dispersion dependencies of LA and TA phonon branches, even at relatively high quasi-wave-vectors.

Atomic structure of the 'cross-linked' PE crystallizes '…in an *orthorhombic* (*Pnam*) phase…at room temperature and atmospheric pressure…' [39, 50]. The c_{KL} matrix for the orthorhombic crystals comprises *9 independent* non-zero elements [55, 56]:

$$c_{IK} = \begin{bmatrix} c_{11} & c_{12} & c_{13} & 0 & 0 & 0 \\ c_{12} & c_{22} & c_{23} & 0 & 0 & 0 \\ c_{13} & c_{23} & c_{33} & 0 & 0 & 0 \\ 0 & 0 & 0 & c_{44} & 0 & 0 \\ 0 & 0 & 0 & 0 & c_{55} & 0 \\ 0 & 0 & 0 & 0 & 0 & c_{66} \end{bmatrix} \quad (16a)$$

The following quantities of the elastic modulus for the *orthorhombic* PE have been evaluated elsewhere in ref. [56]: c_{11} = 15.95 GPa, c_{12} = 6.37 GPa, c_{13} = 2.40 GPa, c_{22} = 15.53 GPa, c_{23} = 5.99 GPa, c_{33} = 362.51 GPa, c_{44} = 6.16 GPa, c_{55} = 3.38 GPa, c_{66} = 6.02 GPa. Numerical 'diagonalization' (using an utility created based on the Octave 3.6.4 freeware) of the Equations (15, 16a) with the listed just above elastic constants and at ρ_M = 950 kg/m^3 [50] yields the following 'components' of the sound velocities of the orthorhombic PE: c_{t1} = 1886.24 m/s, c_{t2} = 2517.31 m/s, and c_l = 4097.50 m/s (with the c_{eff} = 2560.93 m/s) for the <100>-oriented 'cross-linked' crystalline PE; thus, obtained c_{t1x}, c_{t2}, and c_{eff} quantities are *not deviating* vastly from the c_s = 2142 ± 2 m/s reported elsewhere in ref. [50], and implemented at simulations on $C_v(T)$ and $C_p(T)$ dependencies of the *linear* PE, revealed in the Figures 10(a), 10(b).

However, for the <111>-oriented 'cross-linked' PE, c_{t1} = 2219.59 m/s, c_{t2} = 3674.46 m/s, and c_l = 11433.86 m/s (with c_{eff} = 3703.05 m/s) are obtained via the numerical 'diagonalization'. Thus, an alteration in the crystalline orientation of orthorhombic crystalline PE causes quite significant changes in its longitudinal, transverse(s), and effective sound velocities. It is noteworthy that the CM expressed by Equation (16a) is actually obtained under the assumption of essential (spatial) *uniformity* of the *single-crystalline* media within the entire volume of the (non-disrupted) LA and TA phonon propagation (coherence).

However, real atomic structure and morphology of the samples of 'cross-linked' PE might deviate considerably from those of the 'idealized' (i.e., essentially *single-crystalline* in this particular case) *orthorhombic* phase of the PE [57]. Indeed, the atomic structure of real samples of PE would rather be 'composed' of a set of uniform 3D fragments (morphological units) of the orthorhombic crystal structure, *separated* by their grain boundaries, amorphous inclusions ('tissues'), voids, dislocations, etc. [57, 58]. Furthermore, even crystalline orientation(s) of the neighboring 3D fragments (morphological units) might 'fluctuate' considerably [57, 58]. In such a case, the so-called '*orthotropic*' representation of atomic structure(s) of real spatially non-homogeneous materials (including polymeric ones) is often used rather than the approximation of just (uniformly) *anisotropic* media [57]. The 'orthotropic' approximation presumes that actual properties of (really

anisotropic and-essentially-spatially *non-homogeneous*) materials might be represented systematically by just *three* mutually orthogonal spatial directions. In contrast, those properties of *anisotropic* materials may generally vary in different spatial directions, which are *not* necessarily *mutually orthogonal, as* in *the* case of *orthorhombic* and *hexagonal* crystals [28, 44, 46].

Nevertheless, the CM formalism still could be used for *quantitative* evaluation(s) on the *effective* sound velocities of those solids in just 3 mutually orthogonal spatial directions [57, 59]. However, the *structure* of the stiffness (elasticity) matrix, expressed by Equation (16a) for the case of the orthorhombic crystals [55, 56], would be (somewhat) *different*, with just 5 independent non-zero elasticity moduli (constants) [58]:

$$c_{IK} = \begin{bmatrix} c_{11} & c_{11}-2c_{66} & c_{13} & 0 & 0 & 0 \\ c_{11}-2c_{66} & c_{11} & c_{13} & 0 & 0 & 0 \\ c_{13} & c_{13} & c_{33} & 0 & 0 & 0 \\ 0 & 0 & 0 & c_{44} & 0 & 0 \\ 0 & 0 & 0 & 0 & c_{44} & 0 \\ 0 & 0 & 0 & 0 & 0 & c_{66} \end{bmatrix} \qquad (16b)$$

Latter CM corresponds to so-called 'transversely isotropic media', which is (presumably) *axisymmetric* about *z* axis only [57, 59]. In general, elastic modulus (constants) of the CM, suitable for the 'orthotropic' approximation-as well as those incorporated into Equation (16b) in particular-are somewhat *different* as compared to their counterparts, customarily used for the CM of spatially *uniform* (though *anisotropic*) solids even when they are (almost always) denoted by the same symbols [57-59]. Nevertheless, as a 'zero-order' approximation, we may presume that the quantities of all 5 elasticity modules embedded in Equation (16b) are just (pair-wise) equal to their (appropriate) counterparts, incorporated into Equation (16a). Consequently, numerical 'diagonalization' of the 'orthotropic' CM, with the elasticity (stiffness) matrix, expressed by the Equation (16b) yields: c_{t1} = 2517.31 m/s, c_{t2} = 2546.41 m/s, and c_l = 4097.50 m/s (with c_{eff} = 2901.32 m/s) for the <100>-oriented 'cross-linked' crystalline PE. Thus, only c_{t1} and c_{eff} quantities are changed for the orthotropic case as compared to the sound velocities, evaluated via implementation of the Equations (15, 16a) for the <100>-oriented orthorhombic crystal within framework of such approximation, while the c_{t1} and c_l quantities remain the *same* for both orthorhombic and orthotropic approximations (cases).

Now, the $C_v(T)$ and $C_p(T)$ dependencies might be simulated based on Equation (12) for both *orthorhombic* and *orthotropic* modifications of 3D PE. The Figures 11(a), 11(b), compares results of implementation of the basic *anisotropic* equation of the 3D GSM for simulation on the temperature-dependent *harmonic* (in Figure 11(a)) and *anharmonic* (Figure 11(b)) fractions of the lattice thermal capacity of the 'high-density polyethylene' (HDPE) with the experimental $C_p(T)$ dependencies reported elsewhere in refs. [14, 60].

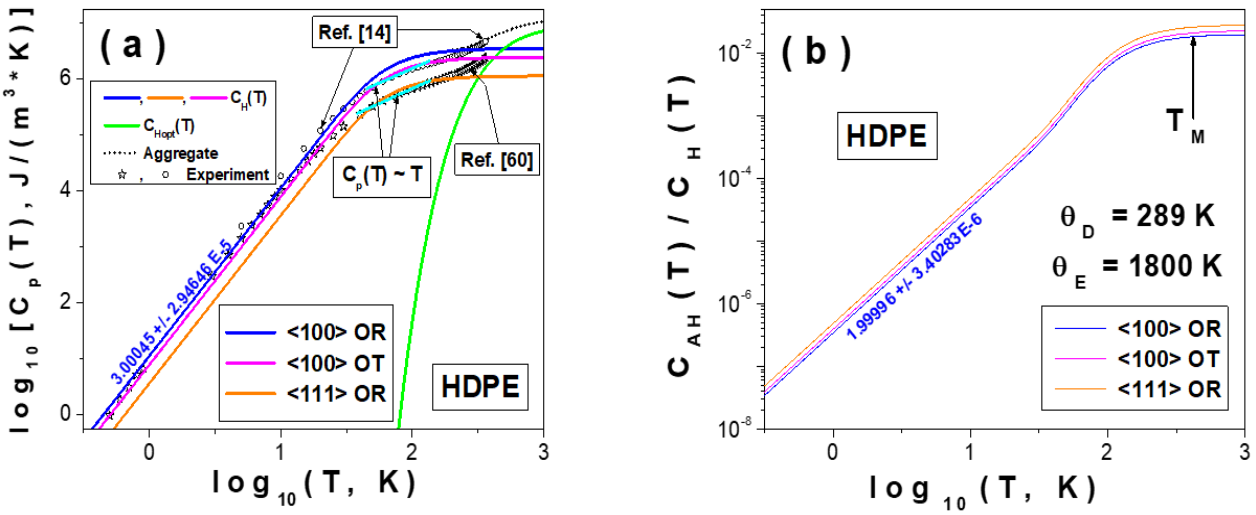

Figure 11 (color online). The *experimental* data were replicated from Refs. [14, 60] (open symbols) and *simulated* (curves)-based on Equation (12) from the previous section-temperature dependences of the **(a)** *harmonic* and **(b)** ratio(s) of the *anharmonic* to the *harmonic* fractions of the lattice thermal capacities of HDPE, evaluated for different crystalline orientations using sound velocities for 3 mutually orthogonal spatial directions, obtained via implementation of the orthorhombic (OR) and orthotropic (OT) CMs: see Equations (15-16b). The contribution from *group vibrations* (optical phonons) is taken into account as well: see *green* curve in the left panel. The log-log slopes of some (low-temperature) $C_H(T)$ and $[C_{AH}(T)/C_H(T)]$ dependencies have been evaluated using standard least-squares procedures and indicated with the blue symbols near the appropriate curves in Figures **(a)** and **(b)**. Vertical arrow in the right panel indicates the *melting temperature* of the crystalline PE (T_M = 414.6 ± 0.5 K), reported elsewhere in ref. [60]. See the main text for more details.

All simulation results are obtained at the *same* (fixed) *sizes* of the *cubical* (in this particular case) phonon confinement volume, i.e., at $L_x = L_y = L_z$ = 1.0 μm, but for 3 different sets of the (an-isotropic in general) sound velocities, evaluated (based on Equations (15-16b)) and listed above in this section of the cases of <100>- and <111>-oriented orthorhombic PE, as well as of <100>-oriented 'orthotropic' PE. Contribution(s) from the *group vibrations* (optical phonons) are also taken into account in Figure 11(a). The latter contributions are evaluated based on a 'truncated version' of the fundamental equation 3D GSM: i.e., Equation (12), in the previous section. In particular, this version corresponds merely to the N = 1 and $E_T = \hbar\omega_{grp} = \hbar\omega_{opt}$ (here $\hbar\omega_{grp}$ and $\hbar\omega_{opt}$ stand for the energies of the 'group vibrations' and optical phonon, respectively); thus, neither summation over different numbers of quasi-particles nor integration over single-particle vibrational spectrum of the acoustic phonons is required for this 'truncated' version of Equation (12). The fixed θ_D = 289 K [53] and θ_E = 1800 K [8] quantities are used in the simulations on the $C_p(T)$ dependencies, revealed in Figure 11(a). The latter temperature matches fairly well with that of the 'wagging' vibrations of the CH_2 group of polyethylene (ranging from 1698.3 K to 1976.6 K), suggested elsewhere in ref. [2]. It is noteworthy that all our simulation results remain significant only for the temperatures *below* the *melting temperature* of crystalline PE, which is indicated with the vertical arrow in Figure 11(b). Indeed, as it is demonstrated in Figures 9(a), 9(b) for the case of polypropylene (PP), behavior of the

experimental $C_p(T)$ dependencies obtained both for amorphous and crystalline modifications of PP reveal abrupt changes at the 'glass transition' temperature, T_g, of this material, implying apparent inter-relation among structural characteristics of PP and its lattice thermal capacity at elevated temperatures. Therefore, thermal properties of PE at temperatures exceeding its melting temperature, T_M, might deviate significantly from their counterpart for the crystalline PE. Significant alteration might also be expected for the *anharmonic* fraction of the lattice thermal capacity of PE in the vicinity of its 'melting point'. Temperature dependence of this fraction has been evaluated solely for the many-particle *acoustic* components of confined thermal vibrations: it is obtained from Equation (12) at N = 2, …, 25.

In other words, the temperature dependence of the $C_{AH}(T)/C_H(T)$ ratio plotted in Figure 11(b) has been evaluated *without* taking into consideration any contribution from the *group vibrations* (optical phonons), even to the $C_H(T)$ quantities, for this particular case. As it is seen readily from Figures 11(a) and 11(b), amendments in the (anisotropic) sound velocities of the HDPE instead affect the *magnitude* of the simulated $C_H(T)$ and/or $C_{AH}(T)$ dependencies than their generic behavior. Indeed, at the relatively low temperatures (T < 30 K), both experimental $C_p(T)$ and simulated $C_H(T)$ dependencies follow closely to the well-known 'Debye's law', $C_p(T) \propto T^3$ [12] for the 3D bulk solids, see Figure 11(a), though being evaluated in this particular case based on the very first term of Equation (12), which takes into account both quantum and anisotropic (orientation-dependent) effects. Since *sizes* of the (cubical) confinement volume presumed the *same* (fixed) at all our simulations on thermal properties of *solid* polymers, the mentioned above alteration in the $C_p(T)$ magnitudes for PE samples with different crystalline orientations have to be attributed entirely to the affect(s) of anisotropic sound velocities. As it is seen clearly from Figure 11(a), the larger (averaged) sound velocities routinely yield lower $C_p(T)$ magnitudes for the low-temperature ranges. However, at elevated temperatures (T > 320 K), the experimental $C_p(T)$ dependencies, reported elsewhere in refs. [14, 60] and re-plotted in Figure 11(a), apparently *deviate* from the 'saturation' behavior (or purely classical Dulong-Petit law), predicted by the well-known Debye's theory [12] for the temperature range, exceeding Debye's temperature of the material. Indeed, the $C_p(T)$ 'bumps' emerge clearly at temperatures exceeding 400 K for the case of HDPE, Figure 11(a). Appearance of such 'bumps' is routinely attributed to impact from the (terminal) *group vibrations* with the Einsteinian (of δ-like-function) vibrational spectrum [8], similar to that of *non-dispersive optical* phonons. Indeed, as it is shown in the Figure 11(a), combined effect of the canonical $C_H(T)$ dependence, evaluated based on purely 'acoustic contribution' from the Equation (12), and an optical 'fraction' (shown with the *green* curve in this figure), yields fairly reasonable approximation for the experimental $C_p(T)$ dependencies, reported elsewhere in refs. [14, 60]. Moreover, all simulated $C_H(T)$ dependencies plotted in Figure 11(a) reveal (almost) *linear* C_p enlargement with the temperature within the temperature range closely surrounding ~100 K, as it is 'highlighted' with the *cyan* solid straight lines in this figure. Such kinds of linear $C_p(T)$ dependencies are quite common for 3D polymeric solids [8], and customarily attributed to the combined impact of 'skeletal' and 'group' vibrations on the experimental $C_p(T)$ dependencies of those solids [8].

As for the temperature-dependent *ratios* of the *anharmonic* to *harmonic* fraction(s) of the lattice thermal capacity of HDPE, their low-temperature log-log slope emerged to be very close to 2 (see Figure 11(b)), which is generally expected for 3D amorphous and crystalline solids based on predictions of the 3D GSM (see, for instance, some discussion on this issue in the section 5.2 in ref. the [24]). However, there is *no* apparent 'low-temperature anomalies' revealed in Figures 11(a), (b),

neither for the experimental $C_p(T)$ dependencies, nor for their experimental counterparts. The obvious reason for the absence of such anomalies for those simulated curves is the extremely low E_{min} quantity, evaluated based on Equation (12a): $E_{min} \cong 2 * 10^{-5}$ eV (20 μeV) emerges at $L_x = L_y = L_z$ = 1.0 μm. Therefore, based on the familiar $E_{min} = k_BT$ relation, the temperature range where the 'low-temperature anomalies' might be (in principle) observed, is limited (from the top) by the $T \cong 2.3 * 10^{-4}$ K (0.23 mK!), which is more than 3 orders of the magnitude below the left margin of the horizontal axes in the Figures 11(a), 11(b). In other words, though based on 'fully quantum' basic equation of the 3D GSM, the 'low-temperature' anomaly is always expected to emerge for the $C_p(T)$ dependence, evaluated for real 3D solid of limited spatial extents, temperature range of its appearance might be 'shifted' towards extremely low temperatures for the parallelepipedal confinement volume of micrometer-sized spatial extents. It is noteworthy that the $[C_{AH}(T)/C_H(T)]$ ratio saturates in Figure 11(b) at significantly higher (approximately by 200 K) temperature as compared to the temperature of saturation of the $C_H(T)$ dependencies, shown in Figure 11(a). Again, this difference in the saturation temperature(s) of the simulated curves, plotted in Figures 11(a) and 11(b), has to be attributed to higher integration limits for the many-particle (*anharmonic*) terms of Equation (12). As it is mentioned above, contributions from the 'group vibrations' (optical phonons) are *not taken* into account in evaluations on the $C_{AH}(T)$ quantities and the $[C_{AH}(T)/C_H(T)]$ ratio(s). In general, such a contribution might significantly amend the 'high-temperature' behavior of the latter ratio(s), and, in principle, might make it even decline with the temperature at T > 300 K for the case of 'cross-linked' PE.

As for quantitative evaluations on the temperature-dependent *entropy* of the *linear* (i.e., essentially 1D) and *branched* (3D) polyethylene(s), PEs, such simulations could be carried out readily using appropriate *combinations* of Equations (10a-10c, 13) for 1D case(s), and that of Equations (12-12c, 13) for 3D ones. Figures 12(a) and 12(b) compare experimental (open symbols) and simulated (curves) $S_T(T)$ dependencies obtained for both the 1D PE and 3D HDPE. As it is seen readily from those figures, the *combinations* of Equations (10a-10c, 13) yields fairly reasonable approximation at L_z = 5.8 nm for the experimental $S_T(T)$ dependence, tabulated for linear PE elsewhere in the Table 3 of ref. [14]: see the lowest simulated curve in the Figure 12(a). This implies straightforwardly, that presence of fairly strong *spatial confinement*, 'discovered' via the comparison of the experimental and simulated $C_v(T)$ curve for linear PE in Figure 10(a) above, is 're-confirmed' again via the comparison of the experimental and simulated $S_T(T)$ dependencies, shown in the Figure 12(a). Indeed, the aforementioned reasonable approximation for the tabulated $S_T(T)$ dependence is obtained under the assumption that the dominant length of the PE MW in the samples studied elsewhere in ref. [14]. It is just under 6 nm! However *enlargement* in the length of the of the PE MWs would affect considerably the entire shape of the simulated $S_T(T)$ dependencies: the 'low-temperature anomalies' apparently become less 'articulated' with the L_z enlargement, while entire $S_T(T)$ curve approaching a *straight line* for PE MWs of L_z = 100 nm: see Figure 12(a). Such behavior is very similar to that of the simulated $S_T(T)$ dependencies, plotted for the (almost) linear 'chains' of polypropylene, see Figure 8 above. However, the 'standard entropy' of PP is ~2.82 times that of PE. As for the temperature-dependent entropy, $S_T(T)$, of the branched HDPE, it rises with the temperature much faster than that of the linear one: compare Figures 12(a) and 12(b). On the other hand, it increases, but not as fast as the $C_p(T)$ function of 3D solids: compare Figure 11(a) and Figure 12(b).

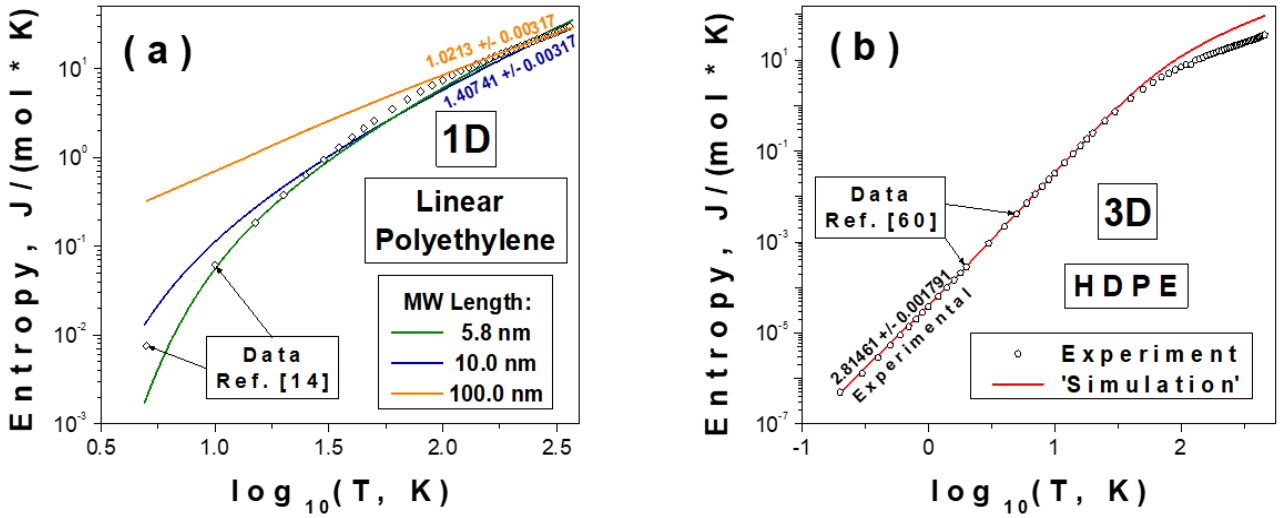

Figure 12 (color online). The *experimental* $S_T(T)$ dependencies (open symbols) are plotted based on data from Tables 3 and 10, given in refs. [14, 60] (respectively), and *simulated* based on *combinations* of equations (10a-10c, 12-12c, 13) from the previous section (curves) for a **(a)** *linear* PE [14] at different MW lengths, and **(b)** 'branched' HDPE [60]. The log-log slope(s) of $S_T(T)$ dependencies, evaluated in the temperature range(s) of 100 K ≤ T ≤ 300 K (for panel **(a)**) and of 0.1 K ≤ T ≤ 5 K (for panel **(b)**) are indicated as well near appropriate curves. See the main text for more details.

In other words, the temperature-dependent *entropy*, $S_T(T) \propto T^{\sim 2.8}$, in Figure 12(b) does *not follows* Debye's 'law', $C_v(T) \propto T^3$, well-established for the *heat capacity* of 3D solids [12]. This deviation apparently originates from the *linear* (in temperature) term embedded in the *denominator* of the 'integrand' of the Eq. (13). In contrast to the results revealed in the Figure 12(a), where both simulated $S_T(T)$ and $C_v(T)$ dependencies have been *re-calculated* (using appropriate Octave 3.6.4 utility) for *every* given *length* of PE MW based on the *combinations* of Equations (10a-10c, 13), the *simulated* curve in the Figure 12(b) is rather obtained by the appropriate 'treatment' of the *experimental* $C_v(T)$ data reported elsewhere in ref. [60], and re-plotted herein in Figure 11(a). In particular, the $[C_v(T)/T]$ ratio evaluated numerically for that data set has been further integrated *numerically* using Origin 8.5 software package, installed on my home computer. As it is seen readily from comparison of the *experimental* dependencies, plotted with the open symbols in the Figure 12(b), with its 'simulated' counterpart (plotted with the *red curve*), both those dependencies are *matching* fairly *well* within the temperature range limited (on its top) with T ≅ 32 K. However, above this temperature, the 'simulated' $S_T(T)$ curve *rises* significantly *faster* with the temperature than its experimental counterpart does. The most evident reason for such behavior is that the original (experimental) $C_v(T)$ dependence, plotted in the Figure 11(a), and thereafter 'treated' (in the explained just above way) to obtain the 'simulated' $S_T(T)$ curve, is impacted significantly at relatively high temperatures by contribution(s) from the *vibration of dangling groups* (see green curve in the Figure 11(a) and comments to it). This high-temperature *deviation* among the experimental and 'simulated' $S_T(T)$ dependencies implies that those 'group vibrations' are *not contributing* significantly to the *entropy* of essentially 3D (orthorhombic) lattice of HDPE (see Figure 12(b)), though yield apparent impact to the $C_p(T)$ dependencies in the Figure 11(a). This discrepancy might

suggest dominant concentration (location) of those relatively intermittent dangling 'groups' on the *periphery* of the 3D structural blocks ('crystals') of the HDPE.

At relatively 'low-temperature' (e.g., at $T \cong 10$ K), the entropy of the 1D (linear) PE is much higher (up to the order of the magnitude!) than that of its 3D HDPE counterpart: compare Figures 12(a), 12(b). This difference probably has to be attributed mainly to the fact that the *orthorhombic* 3D lattice of the HDPE is far more 'rigid' as compared to its 1D counterpart, and the temperature-induced structural disorder is diminished in the 3D spatial arrangement as compared to that in its 1D counterpart. On the other hand, manifestation of the spatial confinement and directly related to it 'low-temperature anomalies' in the 1D polymers with MWs of *limited* (by just *few nano-meters*!) spatial extent *reduces* significantly the *entropy* of 1D lattice at temperatures well below 1 K (where its entropy also emerges well below than that of the low-temperature 3D counterpart) due to essentially 'discretized' vibrational spectrum of 1D polymeric 'chains', and significantly 'suppressed' contribution to the 1D entropy from their vibrational levels of relatively high energy.

Thus, implementation of different versions of the fundamental equations of the GSM, revealed in the previous section, allows one to carry out realistic quantitative simulations on the temperature-dependent *isochoric* (harmonic) and *isobaric* lattice thermal capacity, as well as on *entropy* of *solid* but spatially non-homogeneous polymeric materials with different dominant spatial dimensionalities, topology of their atomic 'networks' and morphology: i.e., for 1D, 2D and 3D 'versions' of those materials-within wide temperature ranges, limited, however, by the temperatures of phase transitions for such solid materials. Alteration (s) in the spatial dimensionality of atomic networking of polymers caused by their phase transitions would affects *directly* crucial features of the experimental and simulated $C_v(T)$ and $C_p(T)$ dependencies. Since all GSM equations include explicitly key *morphological parameters* of solid(s) (polymers) of different spatial dimensionalities and extents, as well as those of their atomic structures, which allows one to evaluate quantitatively effect of alteration(s) in the sizes (volumes) of the phonon confinement area(s) and crystalline orientation of those (if any) on the key features of their temperature-dependent lattice heat capacity and entropy of linear and 'cross-linked' polymers and oligomers composed of structural units of spatially different extent(s), varying in the range from just few nano-meters to (potentially) tenths micro-meters. Therefore, abrupt alterations in the phonon confinement sizes caused (for instance) by the phase transition(s) are generally expected to cause drastic changes in the thermal characteristics of polymers. On the other hand, strong phonon confinement within relatively small (in sizes) linear molecular chains of solid polymers and *oligomers* emerges in an appearance of well-articulated 'low-temperature' anomalies in the $C_p(T)$ dependencies when the chain length (size) diminishes till 5-10 nm, depending on other parameters (molecular weight, Debye temperature, etc.) of polymers: see simulation results and experimental data plotted in Figures 7(a)-12(a). Features of those 'low-temperature' anomalies are linked intimately to the spatial extents (sizes) of the phonon confinement within the polymeric structures and connected directly by quantization ('discretization') of their vibrational spectra. Thus, the appearance of such anomalies becomes unambiguous experimental evidence on the manifestation of phonon confinement(s). When, however, the spatial extent(s) of the confinement rises till micro-meters (and above), those 'low temperature anomalies' might *not* be *manifested* in the $C_p(T)$ and $S_T(T)$ dependencies within the entire temperature range, available for 'routine' measurements: see, for instance, Figures 11(a), 11(b). This, however, does not imply any diminishment in the physical essences of the phonon confinement phenomenon for thermal characteristics of (solid) polymers

with an *arbitrary* spatial extent. Therefore, the phonon confinement is taken into account explicitly in all versions (s) of the basic equation(s) of the GSM, regardless of their dimensionalities and (anticipated) spatial extents: see details in the previous section. On the other hand, the absence of visible 'low-temperature anomalies' might instead encourage additional experimental investigation(s) on essential features of atomic structure and morphology of real polymeric material, to obtain decisive information regarding spatial characteristics (sizes, orientations, etc.) of the thermal vibration of the polymeric solids.

An appropriate combination of fundamental (single-particle) vibrational spectra of the basic equations of the 1D and 3D GSMs might yield a fairly reasonable approximation for the *quantized* ('discretized') and *anisotropic* (if any-for the 3D case) version(s) of the 'three-band' model [18] (see also Figure 4(b) and Figure 5 in the introductory section of this article), which was successfully implemented for decades at simulations on the vibrational characteristics and temperature dependencies of the lattice thermal capacities of various polymeric materials [8, 18]; see also references therein. However, there are some significant *differences* in the physical essences of the original version of the 'three-band' model [18] (see also Figure 4(b) and caption to it for illustration) and a (linear) *combination* of the fundamental equations of the 1D and 3D version(s) of the GSM. First, the original 'three-band' model presumes essentially the *quasi-continuous* spectral distributions for the vibrational DOS function of LA and TA phonons, confined within both 1D and 3D structural fragments of the polymeric material [18]. Secondly, the *non-overlapping* energy ranges corresponding to the acoustic vibrations confined within the 1D and 3D structural fragments are presumed *essentially* within the framework of the original version of the 'three-band' model [18]; see also references therein and Figure 4(b) herein for an illustration.

However, the letter assumption implies straightforwardly an extremely (and-to be honest-*unrealistically*) high '*onset*' energy (or corresponding temperature, θ_3,-see Figure 4(b) and caption to it) for the 1D vibrational spectra of the original 'three-band' model, while a combination of the basic equations of the 1D and 3D GSMs rather corresponds to the (significantly) *overlapped*-in general-but 'discretized' spectra of thermal vibrations (phonons), confined within the 1D and 3D structural fragments. Consequently, the lowest energies (denoted as E_{min} in the previous section) of the two *overlapping* components (bands) of the entire 'discretized' vibrational spectrum within framework of the GSM(s) would be defined via just a *linear combination*(s) of the Equations (10a, 12a) for the 1D and 3D structural fragments of the polymeric material, respectively furthermore, since such spectra are essentially 'discretized' (see Figure 5), even the overlapping area of the vibrational spectra still expected to yield a non-uniformly 'discretized' vibrational spectra for entire fundamental spectra of polymeric material, though with some local 'densification' of quantized vibrational level within the 'overlapped' energy range. In contrast, any overlapping among 1D and 3D continuous spectra of the original 'tree-band' model would yield a 'quadratic' overall $P(\hbar\omega)$ function, shifted upward by the constant (energy-independent) quantity of the 1D component of the vibrational DOS, see Figure 4(b). Similar amendments are expected for overlapping ranges of the vibrational energies, corresponding to Tarasov's equations of different spatial dimensionalities. This would imply straightforwardly an *interaction* among acoustic vibrations of 1D, 2D, and 3D structural fragments within the overlapping energy range. This brings us well *beyond* the framework of the 'canonical' three-band model [18].

On the other hand, due to essentially 'discretized' vibrational spectra of basic equations of both 1D and 3D version of the GSM, even existence of *overlapping* vibrational ranges (bands) of the 1D

and 3D (and customarily spatially separated) structural fragments would *not imply* essential interaction(s) among them, except of relatively rare cases of perfect *coincidence* (resonance) among their vibrational frequencies. Indeed, the quantized (discrete) vibrational frequencies of the confined 1D and 3D vibrations are defined apparently by essentially *different morphologies* of those (spatially separated) 1D and 3D structural fragments, as well as by significantly *different* Equations (10-10c) for the 1D fragments, and Equations (12-12c) for the 3D ones. Therefore, cases of 'perfect coincidence' (resonance) among those vibrational frequencies are expected to be relatively *infrequent*. Subsequently, qualitative impression on essential features of the $C_v(T)$ and $C_p(T)$ functions of-for instance-*polyethylene* with its atomic structure (morphology) composed of spatially separated micro-meter-sized 3D (amorphous and/or crystalline) 'blocks', but linked with the nano-meter-long 1D 'chains' (MWs) might be achieved indeed based on a (linear) combination(s) of the $C_H(T)$ dependencies, exhibited in Figures 9(a)-11(a) above in this section. Furthermore, those simulated $C_H(T)$ dependencies might be used as well in quantitative evaluations on the temperature-dependent *entropy* of polymeric materials: please see Figures 8, 12(a), 12(b)and comments to them above. As it is seen from the Figures 8, 9(a)-12(b), within this temperature range, the 'low-temperature' anomalies might emerge clearly (see also Figures 2(b), 3(a), and 3(b) for experimental evidence on existence of such 'anomalies') for polymeric structures of different spatial dimensionality, and such features of the experimental $C_v(T)$, $C_p(T)$ and $S_T(T)$ dependencies might be replicated convincingly based on an appropriate combination of equations of the different versions of the GSM, and the well-known 'generic' Equation (13). It is noteworthy as well, that corrected version(s) of ('boxed' [8]) 1D, 2D and 3D Tarasov's equation(s), and those of the 'three-band' model might predict appearance of the 'low-temperature anomalies' as well, when the 'onset' frequencies of the acoustic phonons are chosen to be *positive* (non-zeroth). However, those 'onset' frequencies for the different versions of the Tarasov equations are often chosen (or adjusted) 'arbitrary', which would yield *unrealistic* behavior of the simulated 'anomalous' $C_v(T)$ dependencies, while similar frequencies of all basic equations of (different versions) of the GSM are linked straightforwardly to the *actual* morphological features (sizes of phonon confinement, crystalline orientation of the confinement volume-if any, etc.) of the spatially non-homogeneous and low-dimensional amorphous and crystalline polymeric solids. Furthermore, an appropriate combination of the *many-particle* terms of Equations (10a-10c, 12) would allow one to simulate temperature dependencies of the *anharmonic* fraction of the lattice thermal capacities of various polymers composed of structural blocks of different spatial dimensionalities, and-in combination with the 'generic' Equation (13)-would yield valuable information on the temperature-dependent entropy of those polymeric samples. In contrast, neither (different versions) of Tarasov's equations, nor those of the 'mass-weighted velocity' autocorrelation function formalism [39], 'Wigner-Kirkwood expansion' [41, 42], etc., would allow one to evaluate the (truly) *anharmonic* contributions to the lattice thermal capacity quantitatively.

It is noteworthy that the *isochoric* (harmonic) lattice thermal capacity and entropy of 1D and 3D polymers are evaluated entirely based on single-particle (fundamental) states of the confined LA, TA, and optical phonons, depicted by the very first term(s) of the appropriate basic equation of the GSM. In a certain respect, the aforementioned contributions from the fundamental vibrational states of the GSM replicate their counterparts from the 'skeletal' and 'group' thermal vibrations of polymeric structures to their temperature-dependent lattice thermal capacity. Statistical characteristics of *many-particle* (and essentially *anharmonic*) states of the LA and TA phonons are

obtained based on the concept of *many-particle* vibrational density-of-states, introduced by the author of this article in 1995 [47]. This concept might be further generalized using the famous 'Fock space formalism', pioneered elsewhere in ref. [51]. The statistical characteristics of those many-particle states define features of the temperature dependencies of the *anharmonic* lattice capacities of 1D, 2D, and 3D versions of the GSM. Thus, implementation of different versions of the GSM equations brings essentially new insight to understanding as well as more appropriate ways of quantitative evaluations on crucial (*quantized*) features of the single-particle and many-particle density-of-states states of phonons spatially confined within structural fragments of polymeric materials of different spatial dimensionalities, as well as on those of harmonic and especially *anharmonic* thermal capacity, and even entropy of spatially non-homogeneous and low-dimensional polymeric solids. It is important as well that those *anharmonic* fractions of the lattice thermal capacity are evaluated within frameworks of the GSM in profoundly *non-perturbative* ways, via appropriate evaluations of contributions from the many-phonon states and corresponding *many-particle* vibrational DOS functions. In contrast, the '*first-principles*' calculations implemented widely nowadays at quantitative evaluations on the thermal-transport-related properties of bulk and spatially non-homogeneous (though primarily *crystalline*) solids within frameworks of so-called 'Density Functional Theory' (DFT) and/or 'Density Functional Perturbation Theory' (DFPT) one are based essentially on 'perturbative' evaluations of the force constants and other key 'internal' parameters of crystalline materials [61-63].

Furthermore, such evaluations are still extremely *computationally demanding* (even for elementary solids with large numbers of atoms within their unit cells, like beta-modification of *boron*, which comprises of 106 atoms (!) in its unit cell), while non-perturbative approach developed within framework of (different versions) of the GSM allows one to carry out computationally 'non-expensive' and fairly rapid quantitative evaluations on the many-particle VDOS functions and closely related to them *anharmonic* fractions of the lattice capacities of spatially non-homogeneous and low-dimensional solids [23-25, 28, 44]. The *non-perturbative* approach is generally expected to be especially meaningful for 1D cases, like evaluations on vibrational and thermal properties of 'molecular wires'. Moreover, the DFT/DFPT evaluations on vibrational and thermal properties of 'industrial' polymeric materials with a (often *not known* with a sufficient accuracy) *combination* of structural and/or morphological features of fragments of different spatial dimensionalities could be simply computationally *ineffective*, though such evaluations might give very useful inside on specific vibrational and thermal characteristics of unique polymeric 'species', like 'fullerenes', 'cages', etc. Thus, in general, predictions of the (different versions) of the basic (and essentially non-perturbative) equations of the GSM goes well beyond prediction(s) of the well-known Tarasov's equations, those of the 'three-band' model as well as of other theoretical approximation(s), reviewed in the introductory section.

4. Conclusions

In spite of intensive and lasting experimental and theoretical investigations on the features of temperature-dependent thermal capacity of polymers, some crucially important questions remain unanswered. First of all, it is *not established* so far the physical origin(s) behind *sharp decline* in the heat capacity of some linear polymers with the temperature diminishment, or -in other words-actual reasons for appearance of so-called 'low-temperature anomalies': see discussion with examples on

this issue in the introductory section of this article. Secondly, there is *no satisfactory* approach to quantitative evaluations of the truly *anharmonic* contributions to the thermal capacity of polymers, especially of one-dimensional (1D), *linear*, and two-dimensional (2D) ones. To resolve these issues, the 'discretized' version(s) of so-called 'Generalized Skettrup Model(s)' (GSMs) of different (1D, 2D, 3D) spatial dimensionalities are described (see the second section for details) and implemented in the third section of the article at quantitative evaluations on temperature-dependent *harmonic* and *anharmonic* fractions of lattice thermal capacity as well as of the entropy of *linear* polypropylene and polyethylene as well as of those of 'cross-linked' polyethylene with dominant crystalline and/or amorphous atomic structures. Basic equations of all aforementioned versions of the GSM take into account explicitly the *spatial confinement* (within the 1D, 2D and/or 3D structural fragments of those polymers) of conventional longitudinal acoustic (LA), transverse acoustic (TA), and optical phonons and closely related to it *quantization effects* of their *single-particle* (fundamental) and *many-particle* vibrational states, see details in the second section. On the other hand, those equations also imply the *absence* of significant *phonon-phonon interactions* (scattering) within every particular phonon confinement volume, which is, in other words, equivalent to a presumption on the *Casimir limit* for the mean free path of those confined LA, TA, and optical phonons. It is noteworthy that none of the well-known Tarasov's equation(s) (even those with 'boxed' vibrational spectra) take into account appropriately the *spatial confinement* effect. A convincing coincidence with appropriate experimental data reported for aforementioned solid polymeric materials is achieved based on fairly reasonable sets of thermal and acoustic parameters for those 1D and 3D polymers. For instance, experimentally identified 'low-temperature anomalies' of the lattice *thermal capacity* and temperature-dependent *entropy* of *linear* polyethylene and polypropylene are replicated for such polymeric chains (oligomers) at their chain length(s) varying in the range from 2 nm to 10 nm, see simulation results plotted in the previous section. Such 'anomalies' manifest the unambiguously existing strong *spatial confinement* for acoustic and optical vibrations within real solid polymeric materials.

On the other hand, essential features of different versions of the GSM are discussed as well in comparison with those of Tarasov's equations, the well-known 'three-band' model, as well as those of other theoretical approximations, reviewed briefly in the introductory section. *Anisotropic* effects in the *orthorhombic* atomic structure of 'cross-linked' polyethylene are taken into account via evaluation of *anisotropic* sound velocities of conventional thermal waves (acoustic phonons) with linear dispersions, confined within its 3D (poly)crystalline fragments. Such evaluations have been carried out quantitatively via implementation of the Christoffel Matrix (CM) formalism, see details in the second section. similar simulation results were obtained earlier via implementation of the GSM(s) for 1D MWs [28, 44], 2D square flakes [23] and/or rectangular nano-ribbons [25], as well as that of 3D parallelepipedal crystallites [24] with 'convex' borders and (presumably) *well-established* spatial extents (sizes) of all those spatial non-homogeneities. However, the simulation results revealed in the previous section of this article are obtained essentially for polymeric structures of well-*known spatial dimensionalities*, but generally *unknown* actual morphological parameters. In a such situation, meaningful description of ensembles of confined acoustic phonons might be obtained via an appropriate 'averaging' of those characteristics for structural fragments of the *same dimensionalities* (e.g., MWs of the *different* lengths) as well as thermal characteristics of structural fragments of *different* spatial *dimensiona-lities*, i.e., in the 'spirit' of an 'ideology' of the well-known since the canonical 'three-band' model: its basic features are discussed to some extent in the

introductory section herein. Thus, in distin-ction from simulation approaches revealed in previously published articles and books, in general, an appropriate *combination(s)* of the fundamental equations of different versions of the GSM would require for realistic description of statistical characteristics of ensembles of acoustic and optical phonons, confined within structural (atomic) networks of real polymeric materials, as well as at simulations on their temperature-dependent lattice thermal capacities an entropy.

On the other hand, experimentally substantiated information on features of 1D, 2D, and 3D structural and morphological fragments (and/or combination of those) of real polymers would be crucially important for the most straightforward implementation(s) of different versions of the GSM. Such information might be obtained readily using several well-established techniques for state-of-the-art structural and morphological characterization of real polymeric materials, and via continuing efforts in the appropriate implementation of those techniques. These would diminish greatly existing uncertainties in the vital information on actual structural and morphological features of the well-known and newly synthesized polymeric materials. Such information would be critical for appropriately implementing the different versions of the GSM, described in this article.

One of the main disadvantages of the current basic equation(s) of the different versions (s) of the GSM is the essential implementation of (apparently oversimplified) *linear* phonon dispersion relations for all polymeric materials studied in this article. Though, in principle, incorporation of a more realistic *non-linear* (at elevated quasi-wavevectors of phonons) dispersion(s) and corresponding vibrational DOS functions into framework of GSM could be fulfilled readily, such kind of correction(s) might not be carried out based entirely on the parameters of the GSM alone, but would rather require a 'complementary' knowledge on appropriate phonon dispersion parameters, evaluated, for instance, via implementation of the DFT and/or DFPT simulations.

So far, the basic equations of different versions of the GSM as well as those of the CM formalism have been successfully implemented herein at simulations on both harmonic and *anharmonic* thermal characteristics of '*industrial*' polymeric materials: polyethylene and polypropylene. Convincing coincidence achieved for the simulated dependencies with their experimental counterpart(s) inspires implementation of those equations at evaluations on lattice heat capacities of *biopolymers* and other key organic and inorganic materials for biomedical and many other vitally essential applications.

Acknowledgments

All simulation results revealed in this article are obtained with utilities created by its author using *Octave 3.6.4* free software: Copyright©1996-2011 John W. Eaton jwe@octave.org; see also http://www.octave.org.

Author Contributions

Authors of this article wrote *individually* main text of its every section, created 'quantized' versions of all basic equations of the different versions of the 'Generalized Skettrup Model' (GSM), and implemented them at evaluations on the harmonic and *anharmonic* lattice thermal capacities of polymeric structures, designed and programmed utilities for simulations on the temperature dependencies of harmonic and *anharmonic* lattice thermal capacities based on those equations of the GSMs, and carried out all aforementioned simulations for the one-dimensional and three-

dimensional polymers, as well as plotted all simulation results exhibited in the article and created captions to every figure (plot).

Funding

None reported.

Competing Interests

The author declares NO potential conflict of interests.

References

1. Tarasov VV, Yunitskii GA. Theory of heat capacity of chain and layer structures. Zh Fiz Khim. 1950; 24: 111-128.
2. Wunderlich B. Heat capacity of solid polymers. In: Thermal analysis in metallurgy. Pittsburgh, PA: The Minerals, Metals & Materials Society; 1992. pp. 77-91.
3. Schliesser JM, Woodfield BF. Lattice vacancies responsible for the linear dependence of the low-temperature heat capacity of insulating materials. Phys Rev B. 2015; 91: 024109.
4. Pyda M, Wunderlich B. Computation of heat capacities of solid state benzene, p-oligophenylenes and poly-p-phenylene. J Therm Anal Calorim. 1997; 49: 685-692.
5. Zhang G, Wunderlich B. Heat capacity of solid state proteins: I. Thermal analysis. J Therm Anal Calorim. 1997; 49: 823-829.
6. Di Lorenzo ML, Zhang G, Pyda M, Lebedev BV, Wunderlich B. Heat capacity of solid-state biopolymers by thermal analysis. J Polym Sci B Polym Phys. 1999; 37: 2093-2102.
7. Liu D, Zhong C. Modeling of the heat capacity of polymers with the variable connectivity index. Polym J. 2002; 34: 954-961.
8. Wunderlich B. Thermal analysis of polymeric materials. Berlin, Germany: Springer Science & Business Media; 2005.
9. Fultz B. Vibrational thermodynamics of materials. Prog Mater Sci. 2010; 55: 247-352.
10. Mermilliod N, Zuppiroli L, Francois B. Thermal conductivity and specific heat of pure and iodine doped polyacetylene $(CH)_x$. J Phys. 1980; 41: 1453-1458.
11. Umesh G, Wunderlich B. Heat capacity and other thermodynamic properties of linear macromolecules. IV. Polypropylene. J Phys Chem Ref Data. 1981; 10: 1051-1064.
12. Debye P. Zur theorie der spezifischen wärmen. Ann Phys. 1912; 344: 789-839.
13. Gaur U, Wunderlich BB, Wunderlich B. Heat capacity and other thermodynamic properties of linear macromolecules. VII. Other carbon backbone polymers. J Phys Chem Ref Data. 1983; 12: 29-63.
14. Chang SS. Heat capacities of polyethylene from 2 to 360 K. II. Two high density linear polyethylene samples and thermodynamic properties of crystalline linear polyethylene. J Res Natl Bur Stand A Phys Chem. 1974; 78A: 387-400.
15. Tarasov VV. Heat capacity of chain and layer structures. Zh Fiz Khim. 1953; 27: 1430-1435.
16. Tarasov VV. Anisotropic atomic vibrations and the heat capacity of layer and chain structures. Dokl Akad Nauk. 1955; 100: 307-310.

17. Gaur U, Shu HC, Mehta A, Wunderlich B. Heat capacity and other thermodynamic properties of linear macromolecules. I. Selenium. J Phys Chem Ref Data. 1981; 10: 89-118.
18. Hirao K, Soga N. Heat capacity and chemical bond strength of oxide glasses. J Ceram Soc Jpn. 1989; 97: 359-364.
19. Born M, Von Karman T. Uber Schwingungen in Raumgittern. Physik Zeits. 1912; 13: 297-309.
20. Born M, Von Karman T. Zur Theorie der Spezifis chen Waermen. Physik Zeits. 1913; 14: 15-19.
21. Dieter Schlüter A. Mastering polymer chemistry in two dimensions. Commun Chem. 2020; 3: 12.
22. Zhang G, Zeng Y, Gordiichuk P, Strano MS. Chemical kinetic mechanisms and scaling of two-dimensional polymers via irreversible solution-phase reactions. J Chem Phys. 2021; 154: 194901.
23. Ligatchev V. The "Generalized Skettrup Model" and lattice thermal capacity of graphene, h-BN, MoS_2, and WS_2 Flakes. ECS J Solid State Sci Technol. 2020; 9: 093014.
24. Ligatchev V. 'Generalized Skettrup Model' and lattice thermal capacity of spatially non-homogeneous and low-dimensional semiconductors and insulators. London, UK: Lambert Academic Publishing; 2021.
25. Ligatchev V. Size-dependent thermal capacity of graphene nano-ribbons. AIP Adv. 2022; 12: 125010.
26. Thybring EE. Explaining the heat capacity of wood constituents by molecular vibrations. J Mater Sci. 2014; 49: 1317-1327.
27. Abramowitz M, Stegun IA. Handbook of mathematical functions: With formulas, graphs, and mathematical tables. North Chelmsford, MA: Courier Corporation; 1965.
28. Ligatchev V. Harmonic and anharmonic lattice thermal capacities of molecular wires and 0001-oriented cylindrical ZnO nano-wires. J Nanosci Res Rep. 2023; 5: 1-10.
29. Ligatchev V. Polycrystalline and spatially non-homogeneous amorphous semiconductors and insulators. Hauppauge, NY: Nova Science Publishers, Inc.; 2017.
30. Victor AC. Heat capacity of diamond at high temperatures. J Chem Phys. 1962; 36: 1903-1911.
31. Kim T, Ding D, Yim JH, Jho YD, Minnich AJ. Elastic and thermal properties of free-standing molybdenum disulfide membranes measured using ultrafast transient grating spectroscopy. APL Mater. 2017; 5: 086105.
32. Jimenez-Rioboo RJ, Artus L, Cuscó R, Taniguchi T, Cassabois G, Gil B. In-and out-of-plane longitudinal acoustic-wave velocities and elastic moduli in h-BN from Brillouin scattering measurements. Appl Phys Lett. 2018; 112: 051905.
33. Mobaraki A, Kandemir A, Yapicioglu H, Gülseren O, Sevik C. Validation of inter-atomic potential for WS_2 and WSe_2 crystals through assessment of thermal transport properties. Comput Mater Sci. 2018; 144: 92-98.
34. Kharadi MA, Malik GF, Khanday FA, Shah KA, Mittal S, Kaushik BK. Silicene: From material to device applications. ECS J Solid State Sci Technol. 2020; 9: 115031.
35. Da Silva AL, Cândido L, Rabelo JT, Hai GQ, Peeters FM. Anharmonic effects on thermodynamic properties of a graphene monolayer. Europhys Lett. 2014; 107: 56004.
36. Liu K, Yan Q, Chen M, Fan W, Sun Y, Suh J, et al. Elastic properties of chemical-vapor-deposited monolayer MoS_2, WS_2, and their bilayer heterostructures. Nano Lett. 2014; 14: 5097-5103.
37. Zhu B, Liu J, Wang T, Han M, Valloppilly S, Xu S, et al. Novel polyethylene fibers of very high thermal conductivity enabled by amorphous restructuring. ACS Omega. 2017; 2: 3931-3944.

38. Gao H, Menzel TP, Müser MH, Mukherji D. Comparing simulated specific heat of liquid polymers and oligomers to experiments. Phys Rev Mater. 2021; 5: 065605.
39. Martoňák R, Paul W, Binder K. Orthorhombic phase of crystalline polyethylene: A constant pressure path-integral Monte Carlo study. Phys Rev E. 1998; 57: 2425-2437.
40. Horbach J, Kob W, Binder K. Specific heat of amorphous silica within the harmonic approximation. J Phys Chem B. 1999; 103: 4104-4108.
41. Wigner E. On the quantum correction for thermodynamic equilibrium. Phys Rev. 1932; 40: 749-759.
42. Kirkwood JG. Quantum statistics of almost classical assemblies. Phys Rev. 1933; 44: 31-37.
43. Alivisatos AP. Semiconductor clusters, nanocrystals, and quantum dots. Science. 1996; 271: 933-937.
44. Ligatchev V. Harmonic and anharmonic lattice thermal capacities of molecular wires and cylindrical ZnO nano-wires. In: Prime archives in physical sciences. Hyderabad, India: Vide Leaf; 2023. pp. 1-39.
45. Ligatchev V. Size-dependent thermal capacity of graphene nano-ribbons. In: Prime Archives in Physical Sciences. Hyderabad, India: Vide Leaf; 2023. pp. 1-21.
46. Ligatchev V. On nature of Urbach's tail in optical absorption spectrum of nano-crystalline zinc oxide (nc-ZnO). AIP Conf Proc. 2024; 2924: 050002.
47. Ligachev VA. Phonon fluctuations and the pseudodoping effect in inhomogeneous amorphous semiconductors I. The Skettrup model and semiconductor morphology. Phys Solid State. 1995; 37: 1218-1222.
48. Blanc C, Rajabpour A, Volz S, Fournier T, Bourgeois O. Phonon heat conduction in corrugated silicon nanowires below the Casimir limit. Appl Phys Lett. 2013; 103: 043109.
49. Selfridge AR. Approximate material properties in isotropic materials. IEEE Trans Sonics Ultrason. 1985; 32: 381-394.
50. Jordan JL, Rowland RL, Greenhall J, Moss EK, Huber RC, Willis EC, et al. Elastic properties of polyethylene from high pressure sound speed measurements. Polymer. 2021; 212: 123164.
51. Fock V. Konfigurationsraum und zweite Quantelung. Z Phys. 1932; 75: 622-647.
52. Chen Z, Wei Z, Chen Y, Dames C. Anisotropic Debye model for the thermal boundary conductance. Phys Rev B Condens Matter Mater Phys. 2013; 87: 125426.
53. Kim T, Drakopoulos SX, Ronca S, Minnich AJ. Origin of high thermal conductivity in disentangled ultra-high molecular weight polyethylene films: Ballistic phonons within enlarged crystals. Nat Commun. 2022; 13: 2452.
54. Rosenbaum JF. Bulk acoustic wave theory and devices. Norwood, MA: Artech House; 1988.
55. Mouhat F, Coudert FX. Necessary and sufficient elastic stability conditions in various crystal systems. Phys Rev B. 2014; 90: 224104.
56. Barrera GD, Parker SF, Ramirez-Cuesta AJ, Mitchell PC. The vibrational spectrum and ultimate modulus of polyethylene. Macromolecules. 2006; 39: 2683-2690.
57. Kroon M, Andreasson E, Persson Jutemar E, Petersson V, Persson L, Dorn M, et al. Anisotropic elastic-viscoplastic properties at finite strains of injection-moulded low-density polyethylene. Exp Mech. 2018; 58: 75-86.
58. Xu F, Djemia P, Belliard L, Huang H, Perrin B, Zerr A. Influence of elastic anisotropy on measured sound velocities and elastic moduli of polycrystalline cubic solids. J Appl Phys. 2021; 130: 035903.

59. Abell BC, Shao S, Pyrak-Nolte LJ. Measurements of elastic constants in anisotropic media. Geophysics. 2014; 79: D349-D362.
60. Gaur U, Wunderlich B. Heat capacity and other thermodynamic properties of linear macromolecules. II. Polyethylene. J Phys Chem Ref Data. 1981; 10: 119-152.
61. Baroni S, De Gironcoli S, Dal Corso A, Giannozzi P. Phonons and related crystal properties from density-functional perturbation theory. Rev Mod Phys. 2001; 73: 515-562.
62. Lindsay L, Hua C, Ruan XL, Lee S. Survey of ab initio phonon thermal transport. Mater Today Phys. 2018; 7: 106-120.
63. McGaughey AJ, Jain A, Kim HY, Fu B. Phonon properties and thermal conductivity from first principles, lattice dynamics, and the Boltzmann transport equation. J Appl Phys. 2019; 125: 011101.